

Dear Author,

Here are the proofs of your article.

- You can submit your corrections **online**, via **e-mail** or by **fax**.
- For **online** submission please insert your corrections in the online correction form. Always indicate the line number to which the correction refers.
- You can also insert your corrections in the proof PDF and **email** the annotated PDF.
- For fax submission, please ensure that your corrections are clearly legible. Use a fine black pen and write the correction in the margin, not too close to the edge of the page.
- Remember to note the **journal title**, **article number**, and **your name** when sending your response via e-mail or fax.
- **Check** the metadata sheet to make sure that the header information, especially author names and the corresponding affiliations are correctly shown.
- **Check** the questions that may have arisen during copy editing and insert your answers/ corrections.
- **Check** that the text is complete and that all figures, tables and their legends are included. Also check the accuracy of special characters, equations, and electronic supplementary material if applicable. If necessary refer to the *Edited manuscript*.
- The publication of inaccurate data such as dosages and units can have serious consequences. Please take particular care that all such details are correct.
- Please **do not** make changes that involve only matters of style. We have generally introduced forms that follow the journal's style. Substantial changes in content, e.g., new results, corrected values, title and authorship are not allowed without the approval of the responsible editor. In such a case, please contact the Editorial Office and return his/her consent together with the proof.
- If we do not receive your corrections **within 48 hours**, we will send you a reminder.
- Your article will be published **Online First** approximately one week after receipt of your corrected proofs. This is the **official first publication** citable with the DOI. **Further changes are, therefore, not possible.**
- The **printed version** will follow in a forthcoming issue.

Please note

After online publication, subscribers (personal/institutional) to this journal will have access to the complete article via the DOI using the URL: [http://dx.doi.org/\[DOI\]](http://dx.doi.org/[DOI]).

If you would like to know when your article has been published online, take advantage of our free alert service. For registration and further information go to: <http://www.link.springer.com>.

Due to the electronic nature of the procedure, the manuscript and the original figures will only be returned to you on special request. When you return your corrections, please inform us if you would like to have these documents returned.

Metadata of the article that will be visualized in OnlineFirst

ArticleTitle	Examining the impact of the Great Barrier Reef on tsunami propagation using numerical simulations	
--------------	---	--

Article Sub-Title		
-------------------	--	--

Article CopyRight	The Author(s), under exclusive licence to Springer Nature B.V. (This will be the copyright line in the final PDF)	
-------------------	--	--

Journal Name	Natural Hazards	
--------------	-----------------	--

Corresponding Author	Family Name	Thran
	Particle	
	Given Name	Amanda C.
	Suffix	
	Division	Water Research Laboratory, School of Civil and Environmental Engineering
	Organization	University of New South Wales
	Address	Sydney, NSW, 2052, Australia
	Phone	
	Fax	
	Email	m.thran@unsw.edu.au
	URL	
	ORCID	http://orcid.org/0000-0002-0885-3126

Author	Family Name	Brune
	Particle	
	Given Name	Sascha
	Suffix	
	Division	
	Organization	GFZ German Research Centre for Geosciences
	Address	Telegrafenberg, 14473, Potsdam, Germany
	Division	Institute of Geosciences
	Organization	University of Potsdam
	Address	Potsdam, Germany
	Phone	
	Fax	
Email		
URL		
ORCID	http://orcid.org/0000-0003-4985-1810	

Author	Family Name	Webster
	Particle	
	Given Name	Jody M.
	Suffix	
	Division	Geocoastal Research Group, School of Geosciences
	Organization	University of Sydney
	Address	Sydney, NSW, 2050, Australia
	Phone	
	Fax	
	Email	

Fax
Email
URL
ORCID <http://orcid.org/0000-0002-0005-6448>

Author Family Name **Dominey-Howes**
Particle
Given Name **Dale**
Suffix
Division Asia-Pacific Natural Hazards and Disaster Risk Research Group, School of Geosciences
Organization University of Sydney
Address Sydney, NSW, 2050, Australia
Phone
Fax
Email
URL
ORCID <http://orcid.org/0000-0003-2677-2837>

Author Family Name **Harris**
Particle
Given Name **Daniel**
Suffix
Division School of Earth and Environmental Sciences
Organization University of Queensland
Address Brisbane, QLD, 4072, Australia
Phone
Fax
Email
URL
ORCID <http://orcid.org/0000-0002-3275-323X>

Schedule Received 12 May 2019
Revised
Accepted 19 January 2021

Abstract Coral reefs may provide a beneficial first line of defence against tsunami hazards, though this is currently debated. Using a fully nonlinear, Boussinesq propagation model, we examine the buffering capacity of the Great Barrier Reef against tsunamis triggered by several hypothetical sources: a series of far-field, Solomon Islands earthquake sources of various magnitudes (M_w 8.0, M_w 8.5, and M_w 9.0), a submarine landslide source that has previously been documented in the offshore geological record (i.e. the Gloria Knolls Slide), and a potential future landslide source (i.e. the Noggin Block). We show that overall, the Great Barrier Reef acts as a large-scale regional buffer due to the roughness of coral cover and the complex bathymetric features (i.e. platforms, shoals, terraces, etc.) that corals construct over thousands of years. However, the buffering effect of coral cover is much stronger for tsunamis that are higher in amplitude. When coral cover is removed, the largest earthquake scenario (M_w 9.0) exhibits up to a 31% increase in offshore wave amplitude and estimated run-up. These metrics increase even more for landslide scenarios, where they tend to double. These discrepancies can be explained by the higher bed particle velocities incited by higher-amplitude waves, which leads to greater frictional dissipation at a seabed covered by coral. At a site-specific level, shoreline orientation relative to the reef platforms also determines the degree of protectiveness against both types of tsunamis, where areas situated behind broad, shallow, coral-covered platforms benefit the most. Additionally, we find that the platforms, rather than gaps in the offshore reef

structure, tend to amplify wave trains through wave focussing when coral cover is removed from simulations. Our findings have implications for future tsunami hazards along the northeastern Australian coastline, particularly as the physiological stressors imposed by anthropogenic climate change further exacerbate coral die-off and reductions in ecosystem complexity. Therefore, areas that experience a protective benefit by the Great Barrier Reef's platforms could be disproportionately more vulnerable in the future.

Keywords (separated by '-') Coral reef - Tsunami - Great Barrier Reef - Submarine landslide - Earthquake - Numerical simulation

Footnote Information **Supplementary information** The online version contains supplementary material available at <https://doi.org/10.1007/s11069-021-04686-w>.



1 Examining the impact of the Great Barrier Reef on tsunami 2 propagation using numerical simulations

3 Amanda C. Thran¹ · Sascha Brune^{2,3} · Jody M. Webster⁴ ·

4 Dale Dominey-Howes⁵ · Daniel Harris⁶

5 Received: 12 May 2019 / Accepted: 19 January 2021

6 © The Author(s), under exclusive licence to Springer Nature B.V. 2021

7 Abstract

8 Coral reefs may provide a beneficial first line of defence against tsunami hazards, though
9 this is currently debated. Using a fully nonlinear, Boussinesq propagation model, we exam-
10 ine the buffering capacity of the Great Barrier Reef against tsunamis triggered by several
11 hypothetical sources: a series of far-field, Solomon Islands earthquake sources of various
12 magnitudes (M_w 8.0, M_w 8.5, and M_w 9.0), a submarine landslide source that has previ-
13 ously been documented in the offshore geological record (i.e. the Gloria Knolls Slide), and
14 a potential future landslide source (i.e. the Noggin Block). We show that overall, the Great
15 Barrier Reef acts as a large-scale regional buffer due to the roughness of coral cover and
16 the complex bathymetric features (i.e. platforms, shoals, terraces, etc.) that corals construct
17 over thousands of years. However, the buffering effect of coral cover is much stronger for
18 tsunamis that are higher in amplitude. When coral cover is removed, the largest earthquake
19 scenario (M_w 9.0) exhibits up to a 31% increase in offshore wave amplitude and estimated
20 run-up. These metrics increase even more for landslide scenarios, where they tend to dou-
21 ble. These discrepancies can be explained by the higher bed particle velocities incited by
22 higher-amplitude waves, which leads to greater frictional dissipation at a seabed covered
23 by coral. At a site-specific level, shoreline orientation relative to the reef platforms also
24 determines the degree of protectiveness against both types of tsunamis, where areas situ-
25 ated behind broad, shallow, coral-covered platforms benefit the most. Additionally, we find
26 that the platforms, rather than gaps in the offshore reef structure, tend to amplify wave
27 trains through wave focussing when coral cover is removed from simulations. Our findings
28 have implications for future tsunami hazards along the northeastern Australian coastline,
29 particularly as the physiological stressors imposed by anthropogenic climate change fur-
30 ther exacerbate coral die-off and reductions in ecosystem complexity. Therefore, areas that
31 experience a protective benefit by the Great Barrier Reef's platforms could be dispropor-
32 tionately more vulnerable in the future.

33 **Keywords** Coral reef · Tsunami · Great Barrier Reef · Submarine landslide · Earthquake ·
34 Numerical simulation

A1 ✉ Amanda C. Thran
A2 m.thran@unsw.edu.au

A3 Extended author information available on the last page of the article

35 1 Introduction

36 Tsunamis threaten low-lying coastal communities around the world. Coral reef ecosys-
37 tems, many of which are positioned between tsunami source regions and densely populated
38 shorelines (Fig. 1), could provide a broad, cost-effective first line of defence for coastal
39 zones (Ferrario et al. 2014). While field-based studies suggest that coral reefs induce effi-
40 cient energy attenuation in wind waves due to their structural complexity (Sheppard et al.
41 2005; Ferrario et al. 2014; Gallop et al. 2014), a lack of consensus endures surrounding
42 their protectiveness against tsunamis.

43 Following a similar logic, some post-inundation field surveys (Fernando et al. 2005;
44 McAdoo et al. 2011) and modelling studies (Shao et al. 2019) have concluded that, due to
45 their structural complexity, coral reef ecosystems impart similar drag-induced attenuation
46 of wave energy on tsunamis. Other field-based studies (McAdoo et al. 2009; Fritz et al.
47 2011; Gelfenbaum et al. 2011) and modelling work (Kunkel et al. 2006; Yao et al. 2012;
48 Roger et al. 2014) echo these conclusions, but with caveats. For instance, some authors
49 caution that the buffering effect of the reef depends on where the reef is located relative to
50 a coastal community or built asset (McAdoo et al. 2009; Fritz et al. 2011), and that wider
51 reefs, preferably those with an extensive reef flat, appear to dissipate tsunami energy more
52 effectively than narrower fringing reefs (Kunkel et al. 2006; Gelfenbaum et al. 2011; Yao

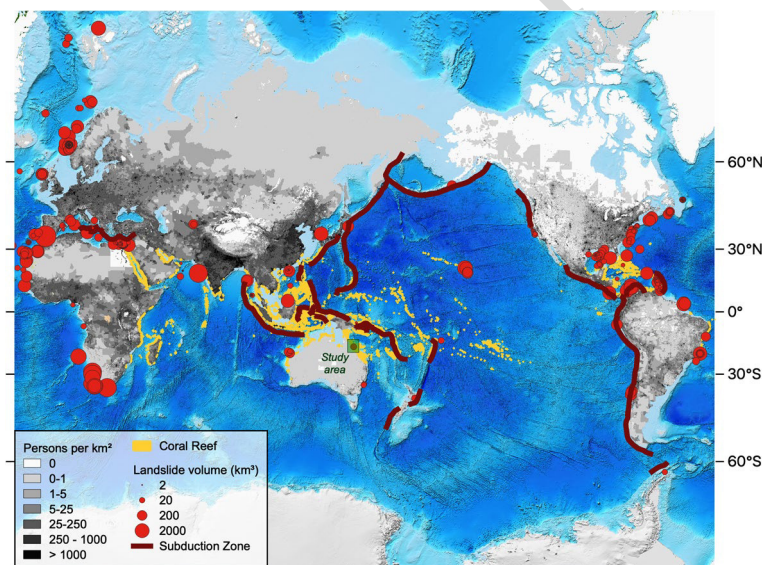


Fig. 1 Global distribution of shallow-water coral reefs (Burke et al. 2011) and their proximity to tsunamigenic sources, including large submarine landslides or landslide complexes ($> 1 \text{ km}^3$; see Online Resource 1 for table of landslide events) and submarine convergent plate boundaries that constitute source zones of major tsunamigenic earthquakes. Landslides are plotted as red circles sized proportionally to the natural log of a given landslide's volume. This compilation is based on several reviews (Hampton et al. 1996; Elverhøi et al. 2002; Owen et al. 2007; Lee 2009; Urlaub et al. 2013; Harbitz et al. 2014; Papadopoulos et al. 2014; Moscardelli and Wood 2016), where landslides with estimated volumes of 1 km^3 were excluded. All original references documenting each of the plotted slides are provided in the reference list of this study. Landmasses are overlaid with gridded UN-adjusted population density for 2020 (CIESIN 2018), with ETOPO1 as the base map (Amante and Eakins 2009)

53 et al. 2012; Roger et al. 2014). Conversely, others have proposed that coral reefs offer mar-
54 ginal to no protective benefit against tsunamis (Baird et al. 2005; Uslu et al. 2010). Further
55 still, some field-based (Nott 1997; Chatenoux and Peduzzi 2005, 2007; Fritz et al. 2011)
56 and modelling work (Roeber et al. 2010; Gelfenbaum et al. 2011; Yao et al. 2012; Ford
57 et al. 2014) suggest that reefs can actually exacerbate damage along neighbouring coast-
58 lines. While there is near-universal consensus that inter-reef passages (or “gaps/openings”
59 between reefs) can amplify tsunami waves, some argue that these amplification effects,
60 along with other effects such as intra-lagoon resonance and increased shoaling/bore forma-
61 tion over shallow reef platforms, undermine any protective benefit that the presence of the
62 reef would otherwise offer (Chatenoux and Peduzzi 2005; Liu et al. 2005; Roeber et al.
63 2010; Gelfenbaum et al. 2011; McAdoo et al. 2011; Ford et al. 2014; Roger et al. 2014).
64 Despite the wide variety of methods and case studies employed to investigate this topic, the
65 impact of coral reef ecosystems on tsunami propagation remains unclear.

66 Ongoing threats to the health and longevity of coral reefs under a changing climate
67 (De’ath et al. 2012; Hughes et al. 2018) heighten these uncertainties. Decades-long field-
68 based studies reveal declines in both coral cover and ecosystem structural complexity as
69 critical reef-building species disappear from coral communities, leading to a progressive
70 “flattening” of reefs (Alvarez-Filip et al. 2009; Bozec et al. 2015; Spalding and Brown
71 2015). It has been proposed that this decline in coral cover will reduce the protectiveness
72 of coral reefs against other common coastal hazards, such as flooding, wind-wave expo-
73 sure (both under fair weather and stormy conditions), and rising sea levels (Quataert et al.
74 2015; Harris et al. 2018; Storlazzi et al. 2018). The literature surrounding the impact of
75 anthropogenically mediated coral decline on tsunami hazards is less conclusive. How-
76 ever, some evidence from post-tsunami field surveys suggests that direct coral removal by
77 means of mining and poaching intensifies tsunami wave heights and inundation extents at
78 a local level (Fernando et al. 2005). In light of recent coral reef decline, and in the wake
79 of recent significant tsunami events (e.g., the 2004 Indian Ocean tsunami, the 2009 South
80 Pacific tsunamis, and the 2011 Tōhoku tsunami), a concerted effort has emerged to more
81 rigorously assess both the present and future coastal buffering role of coral reef ecosystems
82 against tsunamis (Chatenoux and Peduzzi 2007; Ferrario et al. 2014; Spalding et al. 2014),
83 and this study is a contribution to that effort.

84 The Great Barrier Reef (GBR), the world’s largest coral reef system, is an iconic fea-
85 ture of Australia’s coastal landscape. Despite Australia’s proximity to the seismically active
86 source regions (Dominey-Howes 2007; Davies and Griffin 2018), the manner in which
87 tsunami behaviour is regulated by the GBR, which partitions Australia’s coastline from
88 these convergent margins, is not well understood (Webster et al. 2016). Additionally, the
89 discovery of large (volume > 30 km³) landslide scars and slumps on the nearby continental
90 slope (Puga-Bernabéu et al. 2016, 2019) warrants an investigation into the GBR’s ability to
91 protect against landslide-generated tsunamis. Though believed to occur less frequently than
92 their coseismic counterparts, landslide-generated tsunamis such as the 1998 Sissano, Papua
93 New Guinea event (Synolakis et al. 2002) can occur suddenly within close proximity to
94 the shoreline, causing significant localized damage and limiting opportunities for warning
95 and swift response. This, along with the existence of possible paleo-tsunami deposits along
96 the adjacent coastline (Nott 1997), underscores an urgency to quantify the GBR’s widely
97 speculated role as a regional buffer from these hazards (Baba et al. 2008; Puga-Bernabéu
98 et al. 2013a; Wei et al. 2015; Xing et al. 2015; Webster et al. 2016). However, like most
99 coral reefs worldwide, the GBR has not escaped the consequences of anthropogenic cli-
100 mate change (De’ath et al. 2012; Hughes et al. 2018), and therefore, the buffering capacity
101 of the GBR remains uncertain.

102 Thus far, a large portion of the debate surrounding coral reef protectiveness against
103 tsunamis is based on findings from post-tsunami field surveys and anecdotal eye-witness
104 accounts (Baird et al. 2005; Fernando et al. 2005; Liu et al. 2005). However, the degree of
105 a coral reef's influence cannot be quantified solely from these field-based techniques. As
106 many others have highlighted (Chatenoux and Peduzzi 2005; Kunkel et al. 2006; McAdoo
107 et al. 2009; Uslu et al. 2010; Roger et al. 2014; Dilmen et al. 2018), several confounding
108 factors can influence tsunami run-up, such as the extent of coral cover, the nature and prox-
109 imity of the tsunami triggering source, and site-specific variability in coastal bathymetry
110 and topography. Therefore, following a tsunami event, it is difficult to retrospectively ascer-
111 tain the impact of coral reefs in isolation from these other site-specific factors. Numerical
112 simulations can provide additional insights into tsunami behaviour (e.g., Kunkel et al.
113 2006), where experiments can be designed to systematically test the impact of coral cover
114 and reef platform bathymetry on tsunami attenuation while keeping all other parameters,
115 initial conditions, and boundary conditions constant (e.g., Kunkel et al. 2006). Previous
116 studies have aimed to assess the overall impact of the GBR on tsunami propagation using
117 numerical simulations (Baba et al. 2008; Wei et al. 2015; Xing et al. 2015; Webster et al.
118 2016). However, they do not account for smaller-scale structural complexity introduced by
119 coral cover on reef platforms, and they only consider one type of tsunami source at a time.

120 Using numerical modelling, we evaluate the GBR's ability to shield the northeast-
121 ern Australian coastline from a range of hypothetical, though plausible tsunami sources.
122 Firstly, we consider a Solomon Islands earthquake source over various magnitudes (M_w
123 8.0, M_w 8.5, and M_w 9.0). Additionally, we consider two near-field landslide tsunami
124 sources: (1) the largest documented submarine landslide event on the GBR margin (i.e. the
125 Gloria Knolls landslide complex; Puga-Bernabéu et al. 2016), and (2) a potential collapse
126 of a feature on the upper continental slope known as the Noggin Block (Puga-Bernabéu
127 et al. 2013a).

128 In the first of a series of tsunami propagation model runs, for each tsunami source, we
129 numerically simulate the tsunamis assuming healthy coral cover conditions (i.e. "coral-
130 covered platforms" scenarios), where reef platforms are prescribed high roughness to
131 reflect their structural complexity (Nelson 1996). Then, we simulate the tsunamis with
132 smoothed reef platforms (i.e. "smooth platforms" scenarios), where we isolate the impact
133 of live coral cover on wave attenuation (Sheppard et al. 2005). Following the methods of
134 Baba et al. (2008), we further sequester the region's bathymetric complexity by completely
135 excising the reef platforms from the shelf and simulating tsunami propagation with altered
136 bathymetry (i.e. "no reef platforms" scenarios), allowing us to assess the platform-scale
137 buffering capacity of the entire reef structure. We further test the impact of tidal phase
138 on the buffering capacity of the GBR. We then draw upon these findings to consider the
139 broader implications regarding present and future coral reef defence to densely inhabited,
140 low-lying coastal areas.

141 2 Study area

142 2.1 Regional setting

143 The central northeastern Australian margin is a passive margin characterised by a rela-
144 tively broad (~60 km) continental shelf (Fig. 2). The spring tidal range varies from north to
145 south, but the region is generally meso- to macro-tidal (Andrews and Bode 1988). Several

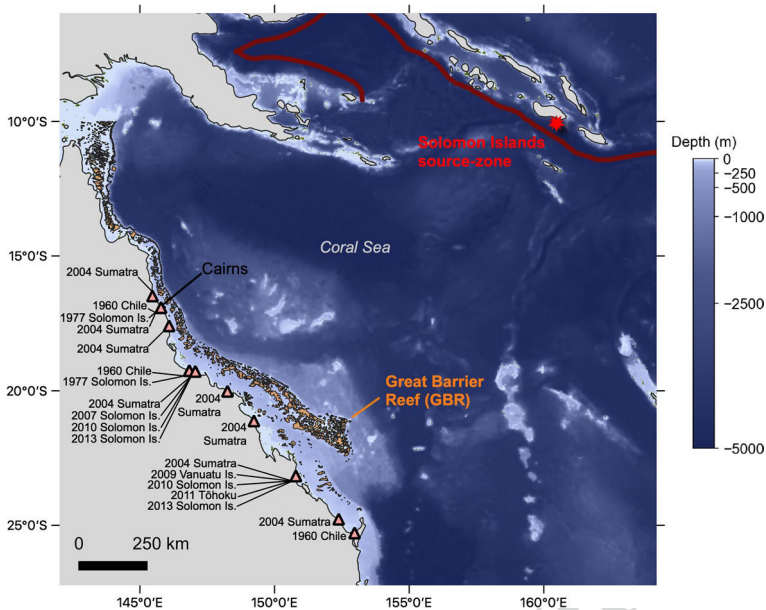


Fig. 2 Regional view of the Solomon Islands source zone, the Coral Sea, and the northeastern Australian margin, which includes the GBR (orange). Also plotted are the locations along the Australian coastline where historical tsunamis that exceeded maximum water heights of 10 cm have been observed using tide gauges (triangles; NGDC/WDS 2020). The red line indicates the subduction zones that traverse the Solomon Islands source zone

146 environmental factors favour coral reef growth on the mid- to outer-continental shelf,
 147 including the region's tropical climate, shallow seas, far proximity from terrestrial run-off,
 148 and nutrient-poor oceanographic conditions. Over hundreds of thousands of years of eus-
 149 tatic sea level fluctuations, these coral reef ecosystems have constructed large (up to ~300
 150 km²) submerged and semi-submerged carbonate platforms, pinnacles, and terraces, which
 151 comprise the offshore reef structure (Hopley et al. 2007; Hinestroza et al. 2016). This reef
 152 structure, which underlies the modern generation of living coral cover, extends roughly
 153 2,300 km along the mid- to outer shelf (Hopley et al. 2007). On the central margin, broad,
 154 arcuate patch reef platforms are separated by relatively wide (up to ~10 km) inter-reef pas-
 155 sages, or "gaps" (Fig. 3). While these passages are wide enough to allow some wind waves
 156 to propagate through to the inner shelf, much of the energy transferred by wind waves is
 157 attenuated atop the reef platforms (Young 1989; Gallop et al. 2014).

158 2.2 Historical and pre-historic tsunami record

159 Historically, northeastern Australia has been affected by tsunamis originating from multi-
 160 ple regions contained within the Pacific Ring of Fire (e.g. Chile, Tonga, and more recently,
 161 Sumatra and Japan; see Fig. 2). Notably, a large proportion of these historical tsunami
 162 events were triggered within subduction zones in the Solomon Islands region, which lies to
 163 the northeast of Australia across the Coral Sea (Dominey-Howes 2007; Australian Bureau
 164 of Meteorology 2020; NGDC/WDS 2020). A nationwide, probabilistic tsunami hazard
 165 assessment revealed that the Solomon Islands source zone poses the greatest hazard to the

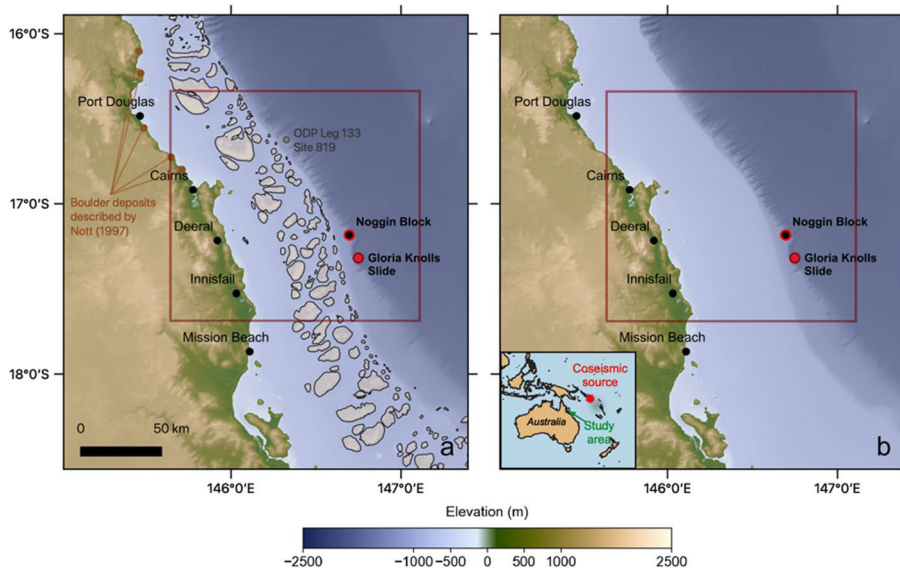


Fig. 3 **a** Bathymetry used in the “coral-covered platforms” and “smooth platforms” simulations. **b** Bathymetry used in the “no reef platforms” simulations. Also shown are the Gloria Knolls Slide, Noggin Block, ODP Leg 133 Site 819, the locations of the boulder deposits described by Nott (1997) and the location of the hypothetical Solomon Islands coseismic sources

166 northeastern Australian town of Cairns and the surrounding area (Davies and Griffin 2018).
 167 Therefore, the Solomon Islands source zone was selected to simulate a range of hypotheti-
 168 cal earthquake-generated tsunami events for this study. In contrast, the pre-historic tsunami
 169 record in northeastern Australia is much more sparse (Dominey-Howes 2007). Nonethe-
 170 less, previous work has described boulder deposits that were speculated to have been
 171 emplaced by tsunami waves (Nott 1997; Fig. 3).

172 2.3 Submarine landslides and areas of potential future collapse

173 Since the collection of high-resolution multibeam bathymetry in 2007 (Webster et al.
 174 2008), a wide variety of submarine landslides have been described on the shelf-edge,
 175 upper, mid, and lower-slope (Puga-Bernabéu et al. 2016, 2019; Webster et al. 2016). These
 176 slides exhibit a range of different sizes and morphologies (e.g. rotational slumps, transla-
 177 tional slides, shovel slides, carbonate terrace collapses, etc.). While they are distributed
 178 along the entirety of the margin, landslides are more commonly found on the north and
 179 central sections of the margin, where the continental slope gradient is moderate to high
 180 (4° – 10° , Puga-Bernabéu et al. 2011, 2013b).

181 The present study focuses on two notable features on the central GBR margin. The first
 182 is the Gloria Knolls landslide complex (Puga-Bernabéu et al. 2016), which is the largest
 183 among the documented submarine landslide cases on the northeastern Australian margin
 184 (total estimated volume $\approx 32 \text{ km}^3$). The entire complex is believed to have failed in mul-
 185 tiple phases, with the estimated age of the first event pre-dating 300 ka (Puga-Bernabéu
 186 et al. 2016). Debris from the slide is visible in both sub-bottom profiles and in bathymetry,
 187 where the debris field extends $\sim 20 \text{ km}$ from the slide scarp. Roughly 8 km northwest of

188 the Gloria Knolls slide complex lies the Noggin Block, a 4.9×3.5 km upper-slope feature
189 that was previously identified as a potential area of future collapse (Puga-Bernabéu et al.
190 2013a). Pockmarks and adjacent landslide scars have also been described around the block
191 (Puga-Bernabéu et al. 2013a). Slope stability modelling indicates that while the block is
192 presently stable, seismic loading could potentially trigger a future failure (Puga-Bernabéu
193 et al. 2013a).

194 We should note that it lies beyond the scope of this work to include a detailed catalogue,
195 and thus a detailed hazard assessment, of landslide tsunami risk on this margin. A com-
196 plete catalogue of all submarine landslides on the GBR margin is currently the subject of
197 future work (Puga-Bernabéu et al., in prep).

198 **3 Methods**

199 **3.1 Tsunami generation**

200 **3.1.1 Earthquake sources**

201 To simulate tsunami generation by an earthquake source, the code Geowave (Watts et al.
202 2003) was used to produce the initial ocean free surface deformation for the hypothetical
203 M_w 8.0, 8.5, and 9.0 coseismic events in the Solomon Islands source zone. Tsunami gen-
204 eration is specifically handled in the TOPICS module of Geowave (Watts et al. 2003). The
205 code incorporates the widely implemented Okada elastic half-space formulation, which
206 relates earthquake geometric source parameters (e.g. fault width, length, strike, dip, etc.)
207 to the initial free surface deformation (Okada 1985). The Okada method has been shown to
208 adequately reproduce free surface deformation for coseismic events exhibiting an abrupt,
209 mostly vertical slip of the seafloor (Kowalik et al. 2005; Fujii et al. 2011) and specifically
210 for past events that originated in the Solomon Islands (Baba et al. 2008). Source param-
211 eters were selected from the Enhanced Tsunami Scenario Database T2 (Greenslade et al.,
212 2009; see Table 1), a suite of earthquake tsunami scenarios developed by the Joint Austral-
213 ian Tsunami Warning Centre and the Centre for Australian Weather and Climate Research.
214 For simplicity, magnitude was altered by modifying the maximum fault slip parameter (see
215 Table 1).

216 **3.1.2 Submarine landslide sources**

217 To simulate tsunami generation by the Gloria Knolls Slide and the potential collapse of
218 the Noggin Block, we used NHWAVE (Ma et al. 2013), a non-hydrostatic wave model that
219 has been successfully validated in laboratory settings (Eneet and Grilli 2007; Tehranirad
220 et al. 2012) and has been used for several case studies of submarine mass failure-induced
221 tsunamis (Tappin et al. 2014; Grilli et al. 2015; Li et al. 2015; Schnyder et al. 2016). The
222 code numerically approximates the solutions to non-hydrostatic Navier–Stokes equations
223 for incompressible flow in three dimensions, implementing a terrain-following (i.e. sigma-
224 layered) vertical coordinate system. For simplicity and computational efficiency, a three-
225 dimensional, rigid, translational failure was assumed for both cases, where the bottom
226 boundary condition is dictated by a time-varying change in depth imparted by an approxi-
227 mately Gaussian-shaped slide.

Table 1 List of input parameters used for tsunami wave generation models.

Hypothetical Solomon Islands earthquake cases		Landslide cases	
		Gloria Knolls slide (worst-case scenario)	Noggin block potential landslide
M_w	8.0	17°19'21.9"S	18°46'48"S
Maximum slip distance (m)	0.8	146°45'07.4"E	148°12'01"E
Centroid latitude	9°50'13.2"S	3947	4900
Centroid longitude	160°37'55.2"E	19,200	3500
Strike (°)	300	288	150
Dip (°)	30	6.51	0.767
Slip rake (°)	90	420	600
Fault length (km)	400	18.6	5.00
Fault centroid depth (km)	10	2000	2000
Fault width perpendicular to strike (km)	80	25.0	25.0
Shear modulus (Pa)	$4.5 \cdot 10^{10}$	0.966	0.280
		Latitude	
		Longitude	
		Length b (m)	
		Width w (m)	
		Maximum thickness T (m)	
		Slide volume (km ³)	
		Initial submergence depth d (m)	
		Mean slope θ (°)	
		Slide density (kg/m ³)	
		Slide terminal velocity (m/s)	
		Initial acceleration a_0 (m/s ²)	

Cases include the hypothetical Solomon Islands earthquake source (M_w 8.0, 8.5, and 9.0 scenarios), the Gloria Knolls Slide, and the Noggin Block potential landslide. Land-slide volumes were calculated using the formulas of Enet and Grilli (2007), which are incorporated into NHWAVE

228 NHWAVE requires approximate landslide dimensions (i.e., length, width, thickness)
229 to construct the Gaussian-shaped slide that generates the initial tsunami. For both land-
230 slide cases, these dimensions were determined in previous work (Puga-Bernabéu et al.
231 2013a, 2016, 2019), and were thus adopted here (see Table 1). For the Gloria Knolls Slide,
232 slide dimensions were determined using bathymetry data containing the slide scar (Puga-
233 Bernabéu et al. 2016, 2019). The slide is believed to have failed sequentially in multiple
234 phases, forming what is known as a larger “slide complex”. Here, we modelled what was
235 determined to be the worst-case scenario of these failure phases (i.e., “Event 2, Worst-Case
236 Scenario”, see Puga-Bernabéu et al. 2019). This case was selected to represent one of the
237 most severe submarine landslide cases for this region, as the Gloria Knolls Slide is, thus
238 far, the largest documented slide complex (total volume $\approx 32 \text{ km}^3$) on the northeastern
239 Australian margin (Puga-Bernabéu, in prep). For the Noggin Block, the initial dimensions
240 were determined from a rigorous, modelling-based slope stability analysis conducted for
241 the block (Puga-Bernabéu et al. 2013a). This feature is comparatively small; the estimated
242 slide volume is $\sim 0.77 \text{ km}^3$ (using the volume formulas of Enet and Grilli 2007). However,
243 the block is relatively shallow, resting on the upper slope ($\sim 400 \text{ m}$). An additional sensitiv-
244 ity analysis was conducted to test the impact of failure depth on the initial tsunami wave
245 height (see Sect. 4.2).

246 For both landslide cases, kinematic parameter a_0 was determined using the semi-empir-
247 ical formulations of Enet and Grilli (2007), and the peak slide velocity was prescribed a
248 value of 25 m/s. This peak velocity is of similar magnitude to those recorded by submarine
249 cable breaks during the Grand Banks Event (i.e., 20–25 m/s; Fine et al., 2005). A landslide
250 density of 2000 kg/m^3 was informed by sediment core measurements obtained by Ocean
251 Drilling Program (ODP) Leg 133 Site 819, which was drilled $\sim 70 \text{ km}$ north of the Nog-
252 gin Block and the Gloria Knolls Slide (Davies et al. 1991). Each simulation was run for a
253 landslide failure duration of 3 min at 100 m resolution horizontally and at 5 sigma layers
254 vertically.

255 3.2 Tsunami propagation

256 The resulting ocean free surface elevations, as well as the depth-averaged zonal and meridi-
257 onal velocities, were smoothed and re-interpolated from the tsunami generation model out-
258 puts to set the initial conditions for the wave propagation model. Tsunami propagation was
259 modelled using FUNWAVE-TVD (Shi et al. 2012), a widely used, fully nonlinear Bouss-
260 inesq tsunami propagation code that has been validated against NOAA’s National Tsunami
261 Mitigation Program benchmark requirements (NTHMP, 2012). The model captures wave
262 behaviours such as shoaling, dissipation via bottom friction and wave breaking, and fre-
263 quency dispersion (Shi et al. 2012).

264 For the earthquake scenarios, tsunami propagation was simulated across the Coral Sea
265 using a 1 arcminute ETOPO1 grid (Amante and Eakins 2009). Smaller nested grids of
266 $200 \times 200 \text{ m}$ resolution were used to resolve the earthquake-generated waves upon arrival
267 to the continental shelf. These grids were generated from a 100 m resolution bathymet-
268 ric dataset spanning the entire northeastern Australian margin, including the GBR (i.e.
269 “3DGBR”, Beaman 2010; see Fig. 3a). Waves were introduced into the smaller nested
270 grids via a one-way coupling scheme. Near-field landslide scenarios were also simulated
271 with grids generated from the 3DGBR bathymetric dataset. Bathymetry for all cases was
272 smoothed using a Gaussian filter to prevent numerical instability incited by steep bathym-
273 etric slopes.

274 The spatial resolution of the model domains was carefully selected using a range
275 of sensitivity analyses (see Online Resource 2). For the earthquake scenarios, a
276 200×200 m grid is deemed sufficient to resolve interactions between the propagating
277 waves and the seafloor. The Gloria Knolls Slide and the Noggin Block potential fail-
278 ure necessitated finer resolution grids to adequately resolve shoaling and scattering pro-
279 cesses (100 m and 50 m resolution, respectively).

280 It is important to note here that although Geowave also has the ability to simulate
281 tsunami generation and propagation by both coseismic slip and landslide sources, we
282 opted to use updated models that more explicitly resolve processes involved in landslide
283 tsunami generation (i.e. the non-hydrostatic formulations of NHWAVE) and more accu-
284 rately represent frequency dispersion of propagating gravity waves (i.e. the improved
285 fully nonlinear, Boussinesq formulations of FUNWAVE-TVD). Dispersive effects
286 become more critical to simulate for far-field and landslide tsunami sources (Tehranirad
287 et al. 2015).

288 3.3 Run-up estimation

289 In the absence of the nearshore high-resolution bathymetric and topographic data (< 50 m)
290 required to accurately resolve onshore tsunami inundation, final estimated run-up distribu-
291 tions were calculated using virtual tide gauges placed along the shoreline in ~25 m water
292 depth d using the following equation:

$$293 R = A(d)^{\frac{4}{5}} \cdot d^{\frac{1}{5}} \quad (1)$$

294 where R is the estimated run-up and $A(d)$ is the maximum wave amplitude at a virtual
295 gauge location at depth d . This formula is based on the conservation of wave energy flux
296 and applies to both breaking and non-breaking waves (Ward and Asphaug 2003).

298 3.4 Testing the impact of the GBR on tsunami propagation

299 A major objective of this study is to test whether the structural complexity of the GBR
300 plays a role in attenuating tsunami wave energy. The GBR exhibits structural complexity
301 at two predominant spatial scales. Firstly, due to the morphological diversity of individual
302 species, coral cover is structurally complex on the meter to sub-meter scale (Nelson 1996;
303 Graham and Nash 2013). We hereafter refer to the structural complexity of coral cover
304 as “ecosystem-scale” complexity. In a modelling context, this “ecosystem-scale” com-
305 plexity cannot be resolved in the computational domain and must be parameterized (see
306 Sect. 3.4.1). Secondly, the GBR exhibits structural complexity at the > 1 km scale. The
307 reef structure itself is composed primarily of completely submerged or semi-submerged
308 carbonate platforms. These features create complex positive relief on the submerged con-
309 tinental shelf, and much of this relief (aside from smaller, deeper pinnacles and terraces)
310 is resolved by the 100 m resolution 3DGBR bathymetric dataset (Beaman 2010). Thus, the
311 reef structure can be adequately resolved in the computational domain. We hereafter refer
312 to complexity introduced by the reef structure as “bathymetric-scale” complexity.

313 The following sections detail how the impact of GBR’s structural complexity at both the
314 ecosystem scale and bathymetric scale was tested.

315 3.4.1 Ecosystem-scale complexity: coral cover parameterization

316 In FUNWAVE-TVD, bottom shear stress τ is calculated using the standard quadratic
317 drag law (Shi et al. 2016):

$$318 \quad \tau = \frac{1}{2} \rho C_D U^2 \quad (2)$$

319 where C_D is the non-dimensional bottom friction coefficient, ρ is the density of water,
320 and U is the particle velocity at the seabed. A variable bottom friction coefficient was
321 established throughout the domain, where it was altered according to the presence or
322 absence of coral cover on reef platforms. A value of $C_D=0.1522$ was prescribed to reef
323 platforms to simulate coral cover (average depth of platforms ≈ 14.9 m). This value was
324 obtained from a prior field investigation of the hydraulic roughness of coral reefs, which
325 was conducted at John Brewer Reef, a reef platform within the GBR that lies close to
326 the study region (Nelson 1996; ~ 80 km from the computational domain). Additionally,
327 this coefficient falls well within the range of values obtained for other reefs (Monismith
328 et al. 2013). All other areas of the computational domain were prescribed the con-
329 ventional value of $C_D=0.0025$, which is representative of sand-covered seafloor (Grilli
330 et al. 2015). This approach was used to create the “coral cover” scenarios, where the
331 ecosystem-scale structural complexity of the GBR was taken into account in tsunami
332 propagation simulations (Fig. 3a).

334 To test the impact of coral cover on tsunami attenuation, the “coral cover” scenarios
335 were then compared to “smooth platform” scenarios, where coral cover was effec-
336 tively removed. In the “smooth platform” scenarios, all areas of the bottom boundary,
337 reef platforms included, were prescribed a standard bottom friction coefficient value of
338 $C_D=0.0025$.

339 3.4.2 Bathymetric-scale complexity: testing the impact of the reef platforms

340 Larger-scale, bathymetric complexity is introduced by the reef structure itself, which is
341 composed primarily of reef platforms. Testing the impact of these platforms on tsunami
342 propagation requires artificial bathymetry, where the positive relief formed by the plat-
343 forms is removed from the shelf (Fig. 3b). Platforms were removed by “cookie-cutting” the
344 bathymetry, removing areas of the mid- to outer-shelf containing the reef platforms. The
345 bathymetry was then linearly interpolated and smoothed over the cookie-cut areas employ-
346 ing a Gaussian filter. This modified bathymetry was then used in the “no reef platforms”
347 scenarios.

348 3.5 Testing the additional effect of tidal phase

349 As the central northeastern Australian margin is a meso-tidal environment, water depths
350 over the reef platforms can vary significantly over several hours. Consequently, tidal phase
351 has been shown to modulate the degree of wind wave attenuation (Young and Hardy 1993).
352 To test the impact of tidal phase on tsunami propagation, two additional scenarios were
353 configured: one where the highest spring tide (+1.75 m above MSL) and one where the
354 lowest spring tide (−1.75 m above MSL) coincided with tsunami arrival at the GBR.

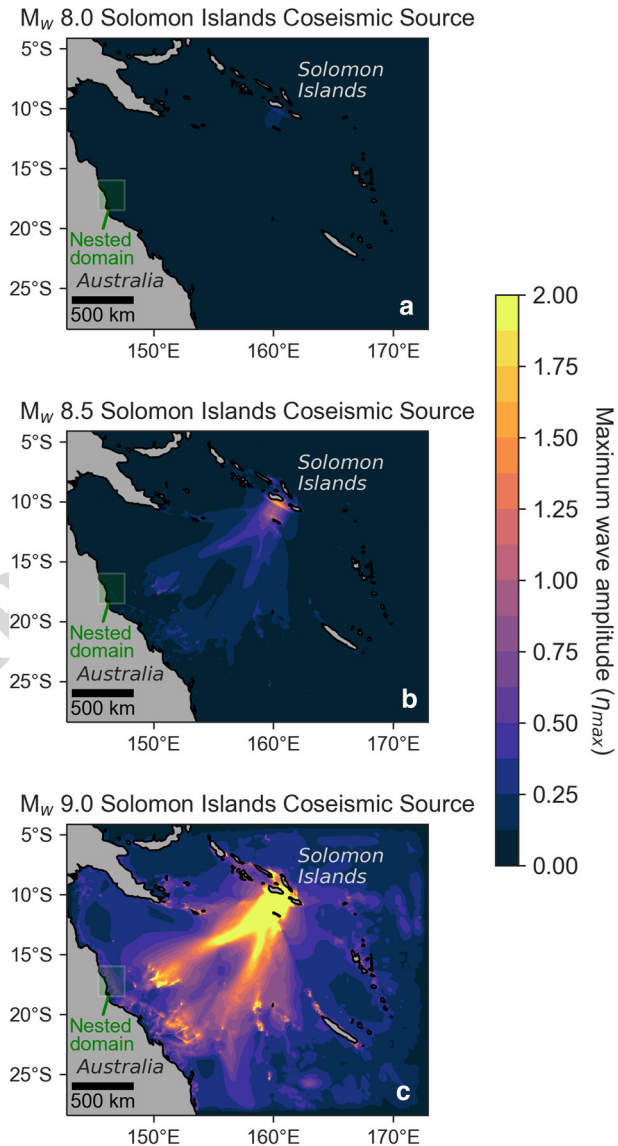
355 **4 Results**

356 **4.1 Earthquake tsunami generation and regional propagation**

357 For the hypothetical M_w 8.0, 8.5, and 9.0 Solomon Islands earthquake scenarios, the gen-
358 eration model simulates initial peak wave amplitudes of 0.32 m, 1.7 m, and 9.7 m, respec-
359 tively (Fig. 4). The tsunamis in each case then propagate across the Coral Sea to the outer
360 GBR margin after an approximately 3.5 h travel time, which is consistent with previous
361 travel times observed for the Solomon Islands source zone (NGDC/WDS 2020). Upon

Author Proof

Fig. 4 Maximum wave amplitudes simulated by FUNWAVE-TVD for the hypothetical M_w 8.0
a, M_w 8.5 b, M_w 9.0 c Solomon Islands earthquake sources. Initial maximum wave amplitudes at the source are 0.32 m, 1.7 m, and 9.7 m, respectively. The simulated propagation time represented here is ~8 h to allow waves to reach all parts of the bathymetric domain



362 arrival to the outer Australian continental shelf within the nested domain, wave amplitudes
363 range from $\sim 1\text{--}2$ cm for the M_w 8.0 case, $\sim 6\text{--}10$ cm for the M_w 8.5 case, and $\sim 30\text{--}60$ cm
364 for the M_w 9.0 case.

365 4.2 Landslide tsunami generation

366 The landslide generation model NHWAVE simulates ~ 18 m-high seaward-propagating
367 wave crest and ~ 9 m-high landward-propagating wave crest for the Gloria Knolls Slide
368 (Fig. 5), assuming the previously determined worst-case scenario (Puga-Bernabéu et al.
369 2019). For the potential collapse of the Noggin Block, the landslide generation model
370 simulates a ~ 1.3 m-high seaward-propagating crest and a ~ 3.5 m-high landward-prop-
371 agating crest (Fig. 6a). Sensitivity analyses indicate that initially generated wave ampli-
372 tudes are responsive to moderate changes in depth (± 100 m). If the block was to initially
373 fail 100 m deeper (500 m depth), the wave amplitude of the landward-propagating crest
374 reaches ~ 2.5 m, about 71% of its original value. On the other hand, should the block fail
375 at a 100 m-shallower depth (300 m depth), the wave amplitude peaks at ~ 4.8 m, grow-
376 ing roughly 37%. For the subsequent simulations of tsunami propagation, the main Noggin
377 Block scenario (failure depth = 400 m) is implemented.

378 4.3 Nearshore earthquake tsunami propagation

379 Results indicate that the GBR's buffering impact on the earthquake-generated tsunami,
380 which originates in the Solomon Islands source zone, depends on the magnitude of the
381 initial earthquake. Turning firstly to the hypothetical M_w 8.0 earthquake scenario (Fig. 7a),
382 maximum wave amplitudes across the domain remain under 5 cm when coral cover is pre-
383 sent atop the reef platforms (i.e. when ecosystem-scale complexity is high), where maxi-
384 mum estimated run-up R_{\max} reaches ~ 6.2 cm. When coral cover is removed (Fig. 7b), max-
385 imum wave amplitudes increase marginally or remain the same, growing 2% on average
386 along the 25 m isobath (Fig. 7c). Estimated run-ups follow a similar trend ($R_{\max} \approx 6.4$ cm).

Fig. 5 Instantaneous free surface elevation at $t=9$ min for the Gloria Knolls landslide tsunami scenario, simulated using NHWAVE. Wave amplitude peaks at $\eta \approx 18$ m. The smaller peak is the landward-propagating wave, and it peaks at $\eta \approx 9$ m

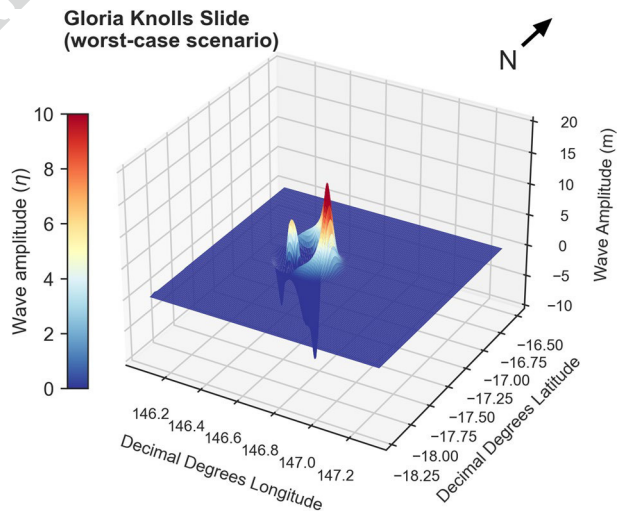
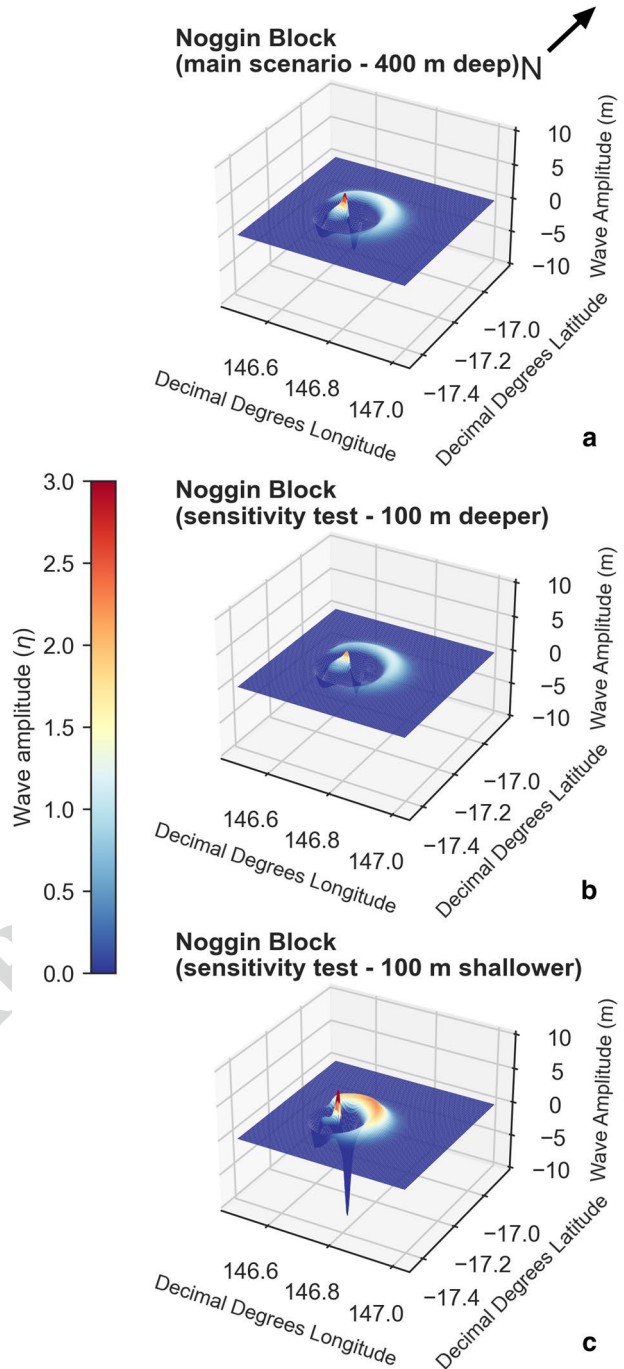


Fig. 6 Instantaneous free surface elevations at $t=9$ min for the potential Noggin Block collapse, simulated using NHWAVE. The main scenario **a** assumes a failure depth of ~ 400 m, where the peak wave amplitude for the landward-propagating crest reaches ~ 3.5 m. A sensitivity test indicates that a 100-m-deeper failure **b** would result in a substantially smaller wave crest ($\eta_{\max} \approx 2.5$ m, 71% of its original value). A 100-m-shallower failure **c** would result in a larger initial wave crest ($\eta_{\max} \approx 4.8$ m, 37% greater than its original value)



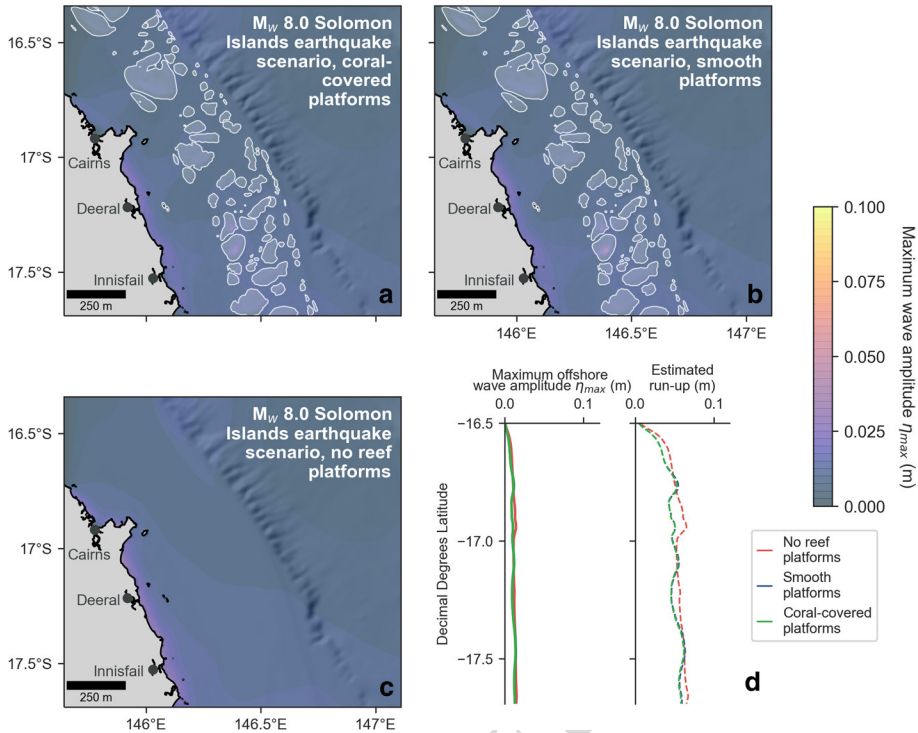


Fig. 7 Maximum wave amplitude distributions for the hypothetical M_w 8.0 Solomon Islands earthquake scenario simulated with **a** the modern “coral-covered platforms” (bottom friction coefficient $C_D=0.1522$ on platforms, shown in white) **b** “smooth platforms” ($C_D=0.0025$), and **c** “no reef platforms”. **d** Corresponding maximum offshore wave amplitude and estimated run-up distributions. Maximum run-up estimates are 6.2 cm for the “coral-covered platforms” scenario, 6.4 cm for the “smooth platforms” scenario, and 6.7 cm for the “no reef platforms” scenario. Offshore wave amplitudes were interpolated along the 25 m isobath

387 Finally, when reef platforms are removed from bathymetry (Fig. 7c), offshore wave ampli-
 388 tudes increase a bit more substantially (17% on average), but still fall below ~ 5 cm across
 389 the domain. The maximum run-up estimate remains at a similar elevation ($R_{max} \approx 6.7$ cm,
 390 Fig. 7d).

391 For the hypothetical Mw 8.5 Solomon Islands earthquake scenario, the GBR, both in
 392 terms of its ecosystem-scale and bathymetric-scale complexity, appears to have slightly
 393 more impact on offshore tsunami amplitudes and estimated run-up. When coral cover is
 394 present (Fig. 8a), wave amplitudes landward of the GBR range from ~ 5 –10 cm, with an
 395 R_{max} estimate of ~ 26 cm. When platforms are smoothed (Fig. 8b), these amplitudes grow,
 396 increasing 7% on average along the 25 m isobath. The maximum run-up estimate also
 397 increases slightly ($R_{max} \approx 28$ cm). Wave amplitudes similarly increase when reef plat-
 398 forms are removed (Fig. 8c; 13% average increase along the 25 m isobath; $R_{max} \approx 32$ cm).
 399 Overall, the changes in the amplitude and run-up distributions are moderate for this case
 400 (Fig. 8d).

401 The GBR has a much more substantial impact on the propagating tsunami when con-
 402 sidering the hypothetical Mw 9.0 Solomon Islands earthquake source. Overall, the Mw
 403 9.0-generated tsunami is significantly larger in amplitude than its smaller-magnitude

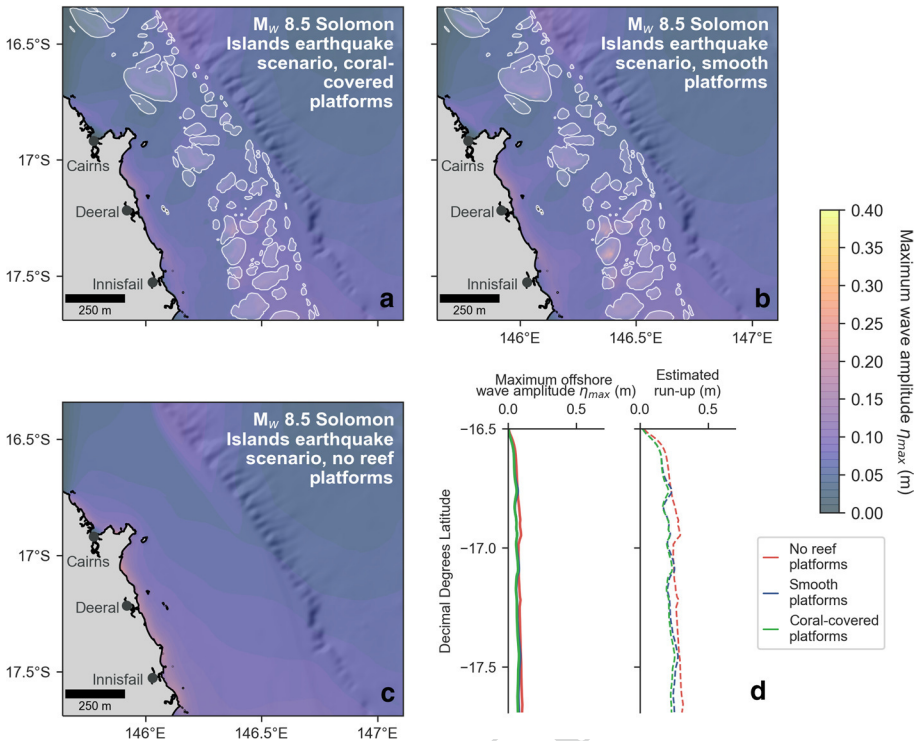


Fig. 8 Maximum wave amplitude distributions for the hypothetical M_w 8.5 Solomon Islands earthquake scenario simulated with **a** the modern “coral-covered platforms” (bottom friction coefficient $C_D=0.1522$ on platforms, shown in white) **b** “smooth platforms” ($C_D=0.0025$), and **c** “no reef platforms”. **d** Corresponding maximum offshore wave amplitude and estimated run-up distributions. Maximum run-up estimates are 26 cm for the “coral-covered platforms” scenario, 28 cm for the “smooth platforms” scenario, and 32 cm for the “no reef platforms” scenario. Offshore wave amplitudes were interpolated along the 25 m isobath. For animations of tsunami propagation for the “coral-covered platforms” and “no reef platforms” scenarios, see Online Resources 3 and 4

404 counterparts. When coral cover is present on reef platforms, maximum offshore wave
 405 amplitudes range from about 0.2–0.4 m landward of the GBR (Fig. 9a), resulting in a
 406 maximum estimated run-up of ~0.85 m. When platforms are smoothed (Fig. 9b), ampli-
 407 tudes increase (18% on average along the 25 m isobath), particularly directly landward of
 408 broad reef platforms. Likewise, the maximum estimated run-up increases when platforms
 409 are smoothed, reaching 1 m. Finally, when reef platforms are removed from bathymetry,
 410 amplitudes increase substantially on the shelf (51% on average along the 25 m isobath),
 411 leading to a maximum estimated run-up of ~1.2 m (Fig. 9d).

412 Figure 10 shows the percentage increase exhibited by both offshore wave amplitude
 413 and predicted run-up when both the ecosystem-scale and bathymetric-scale complexity of
 414 the GBR is removed. This gives an indication of the relative degree to which the GBR
 415 attenuates tsunami wave energy. Firstly, considering ecosystem-scale complexity isolation,
 416 when coral cover is removed, under the Mw 8.0 scenario (Fig. 10a), wave amplitudes are
 417 slightly larger on a percentage-wise basis compared to when coral cover is present, rang-
 418 ing from 0–4% increase within the study area. For the Mw 8.5 scenario, this percentage
 419 increase heightens, ranging from 1–15%. Finally, for the largest earthquake scenario (Mw

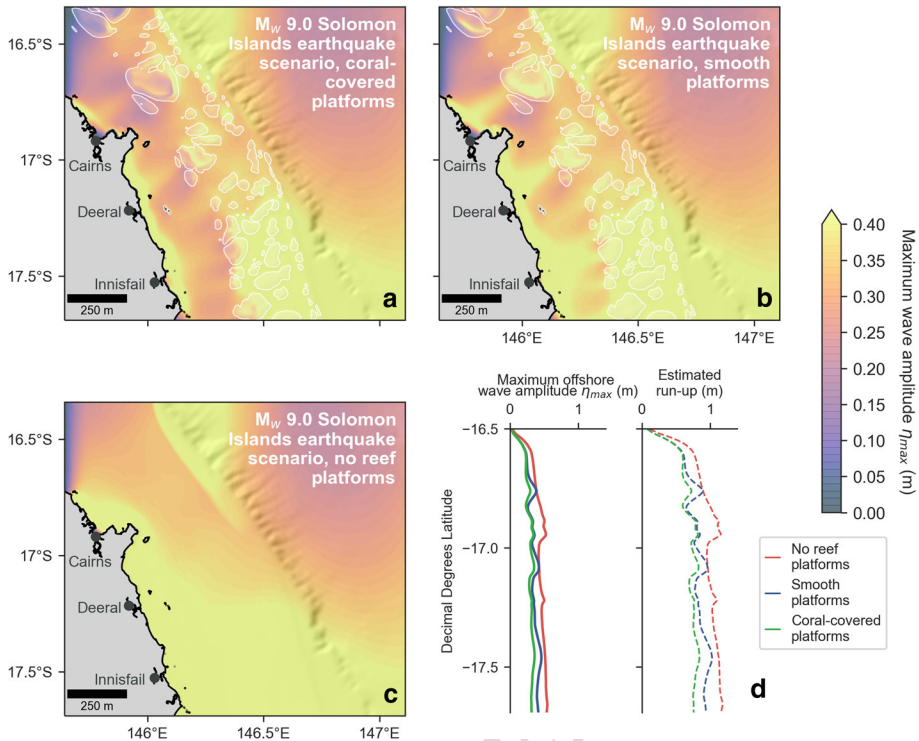


Fig. 9 Maximum wave amplitude distributions for the hypothetical M_w 9.0 Solomon Islands earthquake scenario simulated with **a** the modern “coral-covered platforms” (bottom friction coefficient $C_D=0.1522$ on platforms, shown in white) **b** “smooth platforms” ($C_D=0.0025$), and **c** “no reef platforms”. **d** Corresponding maximum offshore wave amplitude and estimated run-up distributions. Maximum run-up estimates are 0.85 m for the “coral-covered platforms” scenario, 1.0 m for the “smooth platforms” scenario, and 1.2 m for the “no reef platforms” scenario. Offshore wave amplitudes were interpolated along the 25 m isobath

420 9.0), amplitudes increase substantially, ranging from 3–31% higher compared to when
 421 coral cover is present. Percentage increases in the estimated run-up distributions follow
 422 similar patterns. Amplitude and run-up increases are highly variable alongshore, with the
 423 largest peaks occurring directly behind shelf areas with broad, shallow reef platforms. For
 424 instance, the city of Cairns (latitude $\approx 16.8^\circ\text{S}$) seems to benefit from being situated behind
 425 a wide, shallow reef platform that lies in the path of the tsunami. The overall trend indi-
 426 cates that the attenuating effect of coral cover increases with the magnitude of the earth-
 427 quake source.

428 The second panel of Fig. 10 reflects the very substantial combined attenuative impact
 429 of ecosystem-scale and bathymetric-scale complexity (i.e. coral cover and reef plat-
 430 forms). When coral cover and reef platforms are removed, wave amplitudes and run-ups
 431 increase considerably for the M_w 8.0 scenario (range 0–48%). Notably, at a few locations,
 432 this percentage dips marginally below zero (-5% maximum), indicating that these areas
 433 would experience a decrease in offshore amplitudes and estimated run-ups if reef platforms
 434 were not present. Amplitude and run-up distributions follow a similar pattern, increasing
 435 overall for the M_w 8.5 (range 7–70%), and again for the M_w 9.0 (range 20–90%). These
 436 results reflect the significant combined attenuative impact of both coral cover and the reef

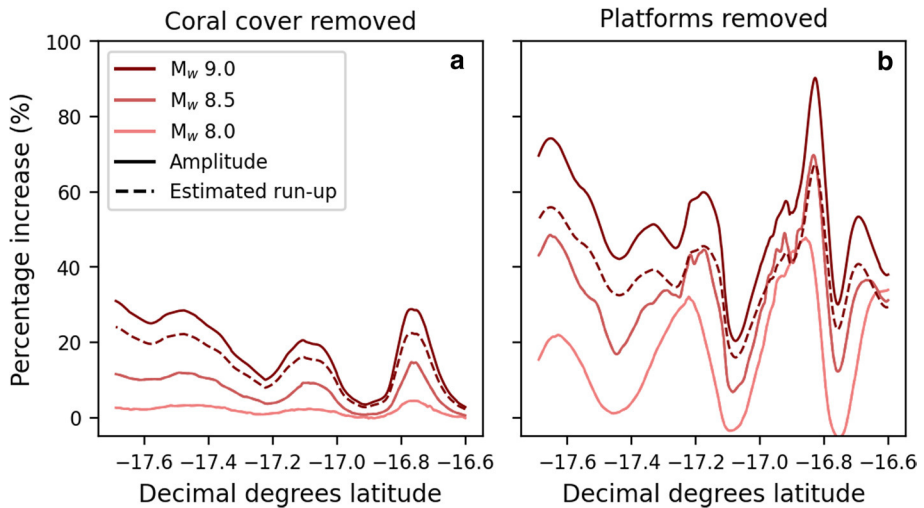


Fig. 10 Percentage increases in both earthquake tsunami amplitude and estimated run-up when **a** coral cover is removed and **b** reef platforms are removed. Amplitudes, which were also used to calculate run-up, were extracted along the 25 m isobath

437 platforms on the propagating tsunamis, which increases with earthquake source magnitude.
438 We again note the immense variability of the amplitude and run-up increases alongshore
439 for each earthquake scenario.

440 For all cases, the first tsunami waves arrive at the coast after an approximately 4 h travel
441 time from the Solomon Islands source zone. When passing over the shelf, the tsunami
442 experiences diffraction, shoaling, and focusing. In particular, broad, moderately deep plat-
443 forms tend to focus tsunami wave energy towards shore (e.g., Fig. 9b). When platforms are
444 removed, this behaviour disappears. For animations of the Mw 8.5 scenario simulated with
445 coral cover and no reef platforms, see Online Resources 3 and 4.

446 4.4 Nearshore landslide tsunami propagation

447 Simulations indicate that the impact of ecosystem-scale and bathymetric-scale complex-
448 ity on tsunami attenuation is sizeable for the landslide-generated cases considered on
449 this margin. Turning firstly to the previously termed “worst-case scenario” for the Gloria
450 Knolls Slide (Puga-Bernabéu et al. 2016), when reef platforms are covered by coral, off-
451 shore amplitudes markedly decline from over ~4 m to under ~2 m landward of the plat-
452 forms (Fig. 11a), and maximum estimated run-up is estimated reaches up to ~2.2 m. When
453 coral cover is removed (Fig. 11b), offshore amplitudes along the 25 m isobath nearly dou-
454 ble, increasing by a factor of ~1.9 on average. Maximum estimated run-up rises to ~3.9 m
455 under the “smooth platforms” simulation. When reef platforms are removed (Fig. 11c), off-
456 shore amplitudes more than quadruple on average (fold change: ~4.6), when compared to
457 the “coral-covered platforms” scenario. When platforms are absent, estimated maximum
458 run-up increases again, reaching 4.6 m (Fig. 11d). The total elapsed time between tsunami
459 generation and the arrival of the first waves is ~1.5 h.

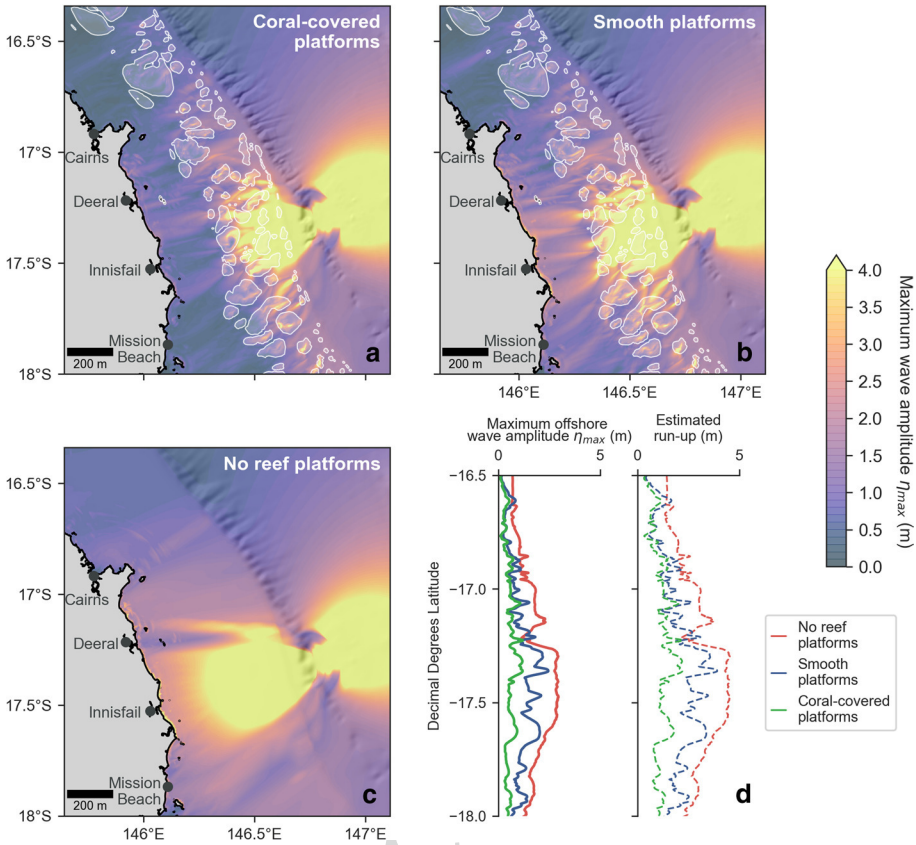


Fig. 11 Maximum wave amplitude distributions for the Gloria Knolls Slide (worst-case scenario) simulated with **a** the modern “coral-covered platforms” (bottom friction coefficient $C_D=0.1522$ on platforms, shown in white) **b** “smooth platforms” ($C_D=0.0025$), and **c** “no reef platforms”. **d** Corresponding maximum offshore wave amplitude and estimated run-up distributions. Maximum run-up estimates are ~ 2.2 m for the “coral-covered platforms” scenario, ~ 3.9 m for the “smooth platforms” scenario, and ~ 4.6 m for the “no reef platforms” scenario. Offshore wave amplitudes were interpolated along the 25 m isobath. For animations of the “coral-covered platforms” and “no reef platforms” scenarios, see Online Resources 5 and 6

460 Results for the Noggin Block potential slide are very similar to that of the Gloria Knolls
 461 Slide, though it produces a smaller tsunami (see Sect. 4.2). Assuming healthy reef growth
 462 (Fig. 12a), offshore amplitudes remain under ~ 1 m, where they sharply decline upon pass-
 463 ing over the GBR platforms. Maximum estimated run-up for this scenario is ~ 1.4 m. When
 464 coral cover is removed (Fig. 12b), offshore amplitudes along the 25 m isobath increase by a
 465 factor of ~ 2 on average, with the maximum run-up rising to 1.8 m. Finally, when platforms
 466 are removed from the simulations (Fig. 12c), offshore amplitudes along the 25 m isobath
 467 are, on average, 4.5 times larger than the original “coral cover” scenario. Peak estimated
 468 run-up reaches ~ 2.8 m under the “no reef platforms” scenario (Fig. 12d). The total time
 469 between tsunami generation and the arrival of the first waves is similar to the Gloria Knolls
 470 landslide tsunami (~ 1.5 h).

471 Figure 10 shows the overall change in offshore wave amplitude and estimated run-up
 472 when coral cover and reef platforms are removed from simulations, this time represented

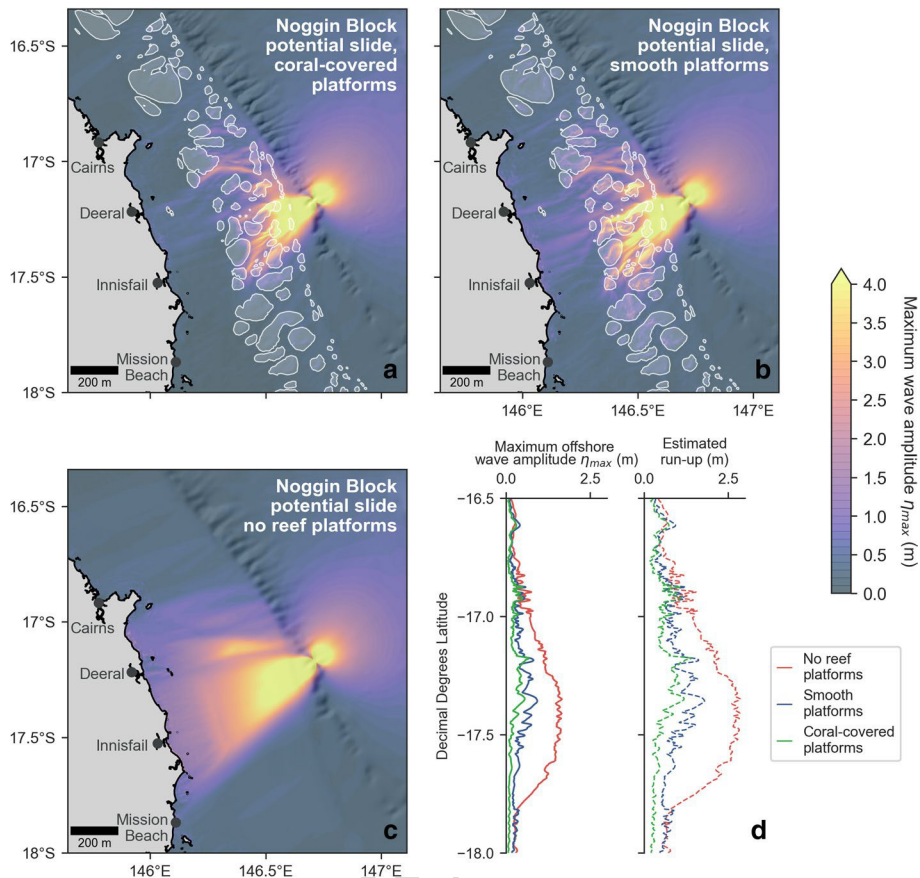


Fig. 12 Maximum wave amplitude distributions for the Noggin Block potential landslide scenario simulated with **a** the modern “coral-covered platforms” (bottom friction coefficient $C_D=0.1522$ on platforms, shown in white) **b** “smooth platforms” ($C_D=0.0025$), and **c** “no reef platforms”. **d** Corresponding maximum offshore wave amplitude and estimated run-up distributions. Maximum run-up estimates are ~ 1.4 m for the “coral-covered platforms” scenario, ~ 1.8 m for the “smooth platforms” scenario, and ~ 2.9 m for the “no reef platforms” scenario. Offshore wave amplitudes were interpolated along the 25 m isobath. For animations of the “coral-covered platforms” and “no reef platforms” scenarios, see Online Resources 7 and 8

473 in terms of fold change rather than percentage change. For each landslide case, offshore
 474 amplitudes along the 25 m isobath, along with estimated run-ups, tend to double when
 475 coral cover is removed (Fig. 10a). When platforms are removed, the amplitudes and run-
 476 ups increase significantly for each case, but more so for the Noggin Block potential slide
 477 (Fig. 10b). Again, we highlight the enormous along-shore variability in amplitude and run-
 478 up change across simulations.

479 Landslide tsunamis across both cases exhibit common behaviours. Amplitude and run-
 480 up distributions follow a localized bell-curve due to radial damping, a standard process
 481 undergone by point-source tsunamis (Brune et al. 2010; Harbitz et al. 2006). Additionally,
 482 reef platforms greatly interfere with these comparably shorter waves as they traverse the
 483 shallow continental shelf (Harbitz et al. 2006). For animations of both the Gloria Knolls
 484 slide scenario simulated with coral-covered platforms and no reef platforms, see Online

485 Resources 5 and 6. For the same corresponding Noggin Block landslide tsunamis, see
486 Online Resources 7 and 8.

487 4.5 Tidal impacts on tsunami propagation

488 The additional impact of tide level was tested for the M_w 8.5 Solomon Islands earthquake
489 scenario, the Gloria Knolls Slide scenario, and the Noggin Block potential slide scenario. **AQ1**
490 Results indicate a minimal impact of tide level on the degree of attenuation of the M_w 8.5
491 earthquake-triggered tsunami (Fig. 13a), where amplitudes were 1.6% lower on average at
492 low spring tide (1.75 m below MSL; Fig. 13b) and 2.6% higher on average at high spring
493 tide (1.75 m above MSL; Fig. 13c). Offshore amplitude and run-up distributions along the
494 25 m isobath are very similar for all tide cases (Fig. 13d). For the Gloria Knolls Slide, the
495 effect of tides is more pronounced, where amplitudes decrease 11% on average during low
496 spring tide and increase 17% on average at high spring tide (Fig. 14). Similarly, for the
497 Noggin Block, potential slide scenario (Fig. 15a), amplitudes were 16% lower on average
498 at low spring tide (Fig. 15b) and 6% higher on average at high spring tide (Fig. 15c).

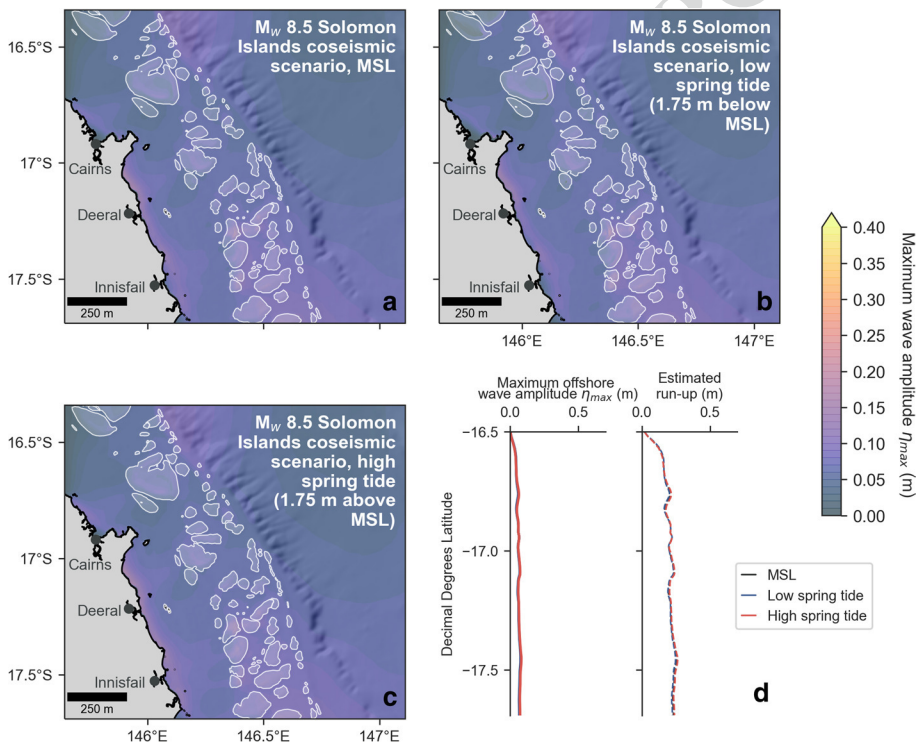


Fig. 13 Maximum wave amplitude distributions for the hypothetical M_w 8.5 Solomon Islands earthquake scenario simulated at a mean sea level (MSL, bottom friction coefficient $C_D=0.1522$ on platforms, shown in white) **b** low spring tide (1.75 m below MSL, $C_D=0.1522$ on platforms), and **c** high spring tide (1.75 m above MSL, $C_D=0.1522$ on platforms). **d** Corresponding maximum offshore wave amplitude and estimated run-up distributions. Maximum run-up estimates are 26 cm for the MSL scenario, 25 cm for the low spring tide scenario, and 26 cm for the high spring tide scenario. Offshore wave amplitudes were interpolated along the 25 m isobath

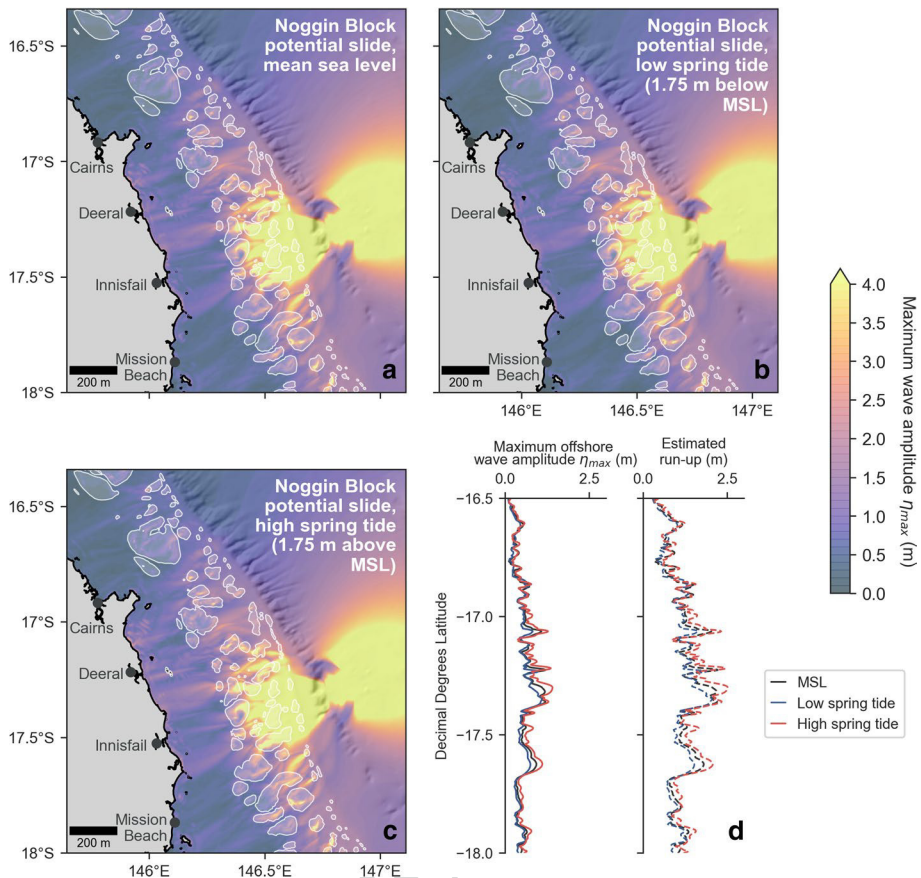


Fig. 14 Maximum wave amplitude distributions for the Gloria Knolls Slide scenario simulated at **a** mean sea level (bottom friction coefficient $C_D=0.1522$ on platforms, shown in white) **b** low spring tide (1.75 m below MSL, $C_D=0.1522$ on platforms), and **c** high spring tide (1.75 m above MSL, $C_D=0.1522$ on platforms). **d** Corresponding maximum offshore wave amplitude and estimated run-up distributions. Maximum run-up estimates are 1.4 m for the MSL scenario, 1.4 m for the low spring tide scenario, and 1.3 m for the high spring tide scenario. Offshore wave amplitudes were interpolated along the 25 m isobath

499 5 Discussion

500 5.1 The impact of the GBR's ecosystem-scale complexity on tsunami propagation

501 Our results show that tsunamis are strongly impacted by the presence of coral cover in
 502 the GBR. Across many of the “coral-covered platforms” simulations, maps showing maxi-
 503 mum wave amplitude distributions show clear “shadow zones” landward of reef platforms,
 504 where amplitudes markedly decrease. These impacts are especially pronounced for the M_W
 505 9.0 Solomon Islands earthquake scenario (Fig. 9), the Gloria Knolls submarine landslide
 506 scenario (Fig. 11) and the Noggin Block potential submarine landslide scenario (Fig. 12).
 507 These declines in wave amplitude are driven by elevated frictional dissipation over coral-
 508 covered reef platforms. We eliminate the possibility that wave breaking contributed to

Natural Hazards

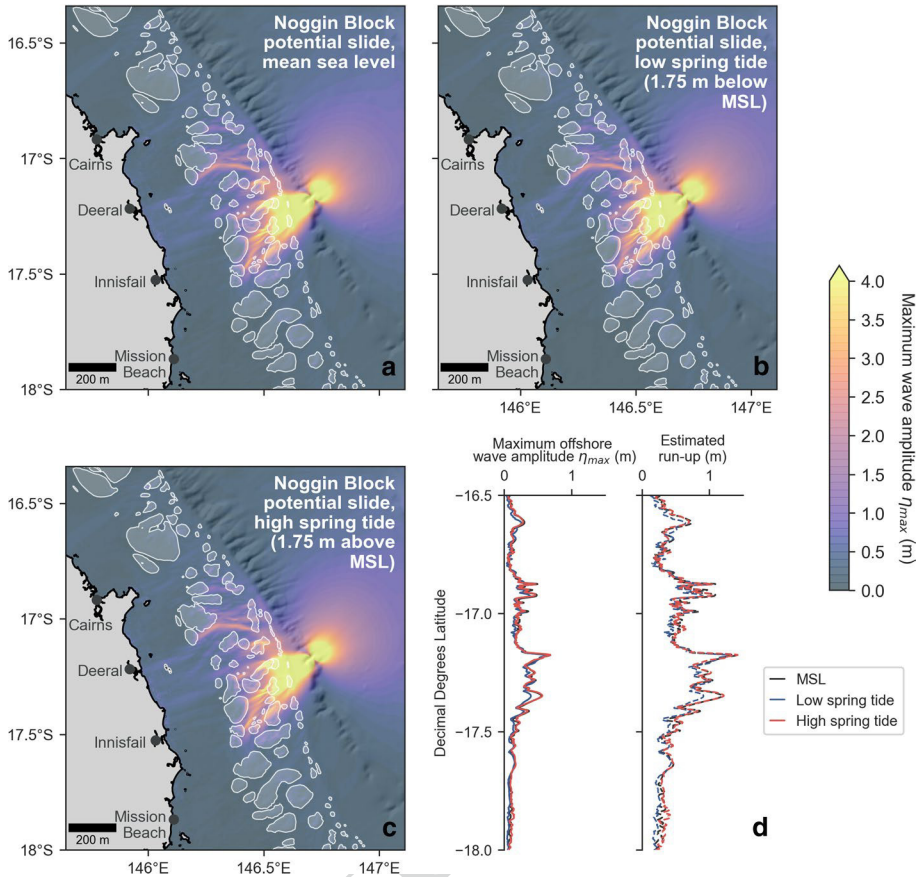


Fig. 15 Maximum wave amplitude distributions for the Noggin Block potential slide scenario simulated at **a** a mean sea level (bottom friction coefficient $C_D=0.1522$ on platforms, shown in white) **b** low spring tide (1.75 m below MSL, $C_D=0.1522$ on platforms), and **c** high spring tide (1.75 m above MSL, $C_D=0.1522$ on platforms). **d** Corresponding maximum offshore wave amplitude and estimated run-up distributions. Maximum run-up estimates are 1.4 m for the MSL scenario, 1.4 m for the low spring tide scenario, and 1.3 m for the high spring tide scenario. Offshore wave amplitudes were interpolated along the 25 m isobath

509 energy dissipation, as wave-breaking was not detected in any of the simulations due to the
 510 tsunamis' large wavelengths in comparison to their amplitudes. These results reaffirm the
 511 prevailing notion that the GBR acts as a regional buffer to tsunamis (Baba et al. 2008;
 512 Wei et al. 2015; Xing et al. 2015; Webster et al. 2016; Puga-Bernabéu et al. 2019). They
 513 are also consistent with previous findings from other modelling studies, especially those
 514 that include wider reef platforms in their assessments (Kunkel et al. 2006; Gelfenbaum
 515 et al. 2011; Yao et al. 2012), which allows the cumulative impact of frictional dissipation
 516 to dominate. Therefore, we propose that the effect of live coral cover should be directly
 517 incorporated into future hazard assessments of the northeastern Australian margin, as we
 518 anticipate it will have a detrimental impact on propagating tsunamis.

519 The energy-diminishing impact of coral cover becomes most apparent when compar-
 520 ing the “coral-covered platforms” simulations with the “smooth platforms” simulations.
 521 When coral cover is removed, amplitudes increase across each source scenario tested here.

522 Notably, run-up projections increase as much as 24% for the M_w 9.0 earthquake source
523 (Fig. 10), and they exhibit a maximum of a nearly fourfold change for the Noggin Block
524 potential slide (Fig. 16). These increases in amplitude and run-up imply that while coral
525 cover in the GBR may currently have a buffering effect on tsunami wave energy, this
526 effect may diminish as reef ecosystems in the GBR continue to decline under the physi-
527 ological stressors (e.g., heat stress, acidity stress) that accompany anthropogenic climate
528 change (Hughes et al. 2018). Generally speaking, the structural complexity of coral reefs
529 is expected to deteriorate as reef-building species are lost and as ecosystems transition to
530 algal-dominated states (Bellwood et al. 2004; Alvarez-Filip et al. 2009; Wild et al. 2011).
531 This deterioration of structural complexity is expected to lessen frictional dissipation of
532 wind wave energy (Harris et al. 2018; de Lalouvière et al. 2020). Based on our results, we
533 expect a similar outlook for tsunami wave hazards. This loss of buffering capacity may be
534 further compounded by the effects of sea level rise, where some assessments have fore-
535 casted heightened tsunami hazard under current projections (Li et al. 2018; Nagai et al.
536 2020).

537 Across source scenarios, there are prominent discrepancies in the magnitude of the
538 amplitude and run-up increases when coral cover is removed. For instance, while the M_w
539 8.0 earthquake scenario experiences marginal increases (4% maximum, see Fig. 10), M_w
540 9.0 scenario experiences substantial jumps in offshore amplitude (up to 31%) when plat-
541 forms are smoothed. This implies that the degree of coral-induced frictional dissipation
542 at bed is different across source scenarios. Our findings demonstrate that these differences
543 in frictional dissipation are directly related to wave amplitude (and thus, wave energy).
544 Particle velocity (note: this is different to wave *celerity*) is a function of wave amplitude
545 (Nielsen 1992), and therefore, waves of differing amplitudes experience different degrees
546 of dissipation due to shear stress at bed. This amplitude-mediated discrepancy in parti-
547 cle velocity is best exemplified by comparing earthquake scenarios, where tsunami ampli-
548 tude was altered by changing the magnitude and slip displacement of the initial coseismic

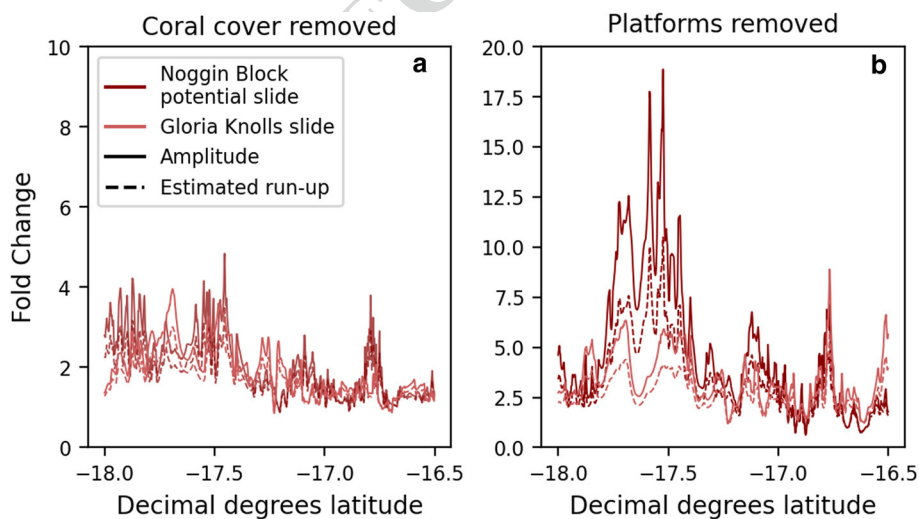


Fig. 16 Fold-change increase in both landslide tsunami amplitude and estimated run-up when **a** coral cover is removed and **b** reef platforms are removed. Amplitudes, which were also used to calculate run-up, were extracted along the 25 m isobath

549 source (Fig. 4, see Table 1 for source parameters). For the M_w 8.0 Solomon Islands earth-
550 quake scenario, bed particle velocities are relatively low (< 1 cm/s) throughout the compu-
551 tational domain given the relatively low tsunami amplitudes produced by the source. How-
552 ever, for the M_w 8.5 and M_w 9.0 earthquake scenarios, particle velocities are much higher
553 on the shelf (> 5 cm/s). Moreover, in their corresponding “smooth platforms” simulations,
554 particle velocities are more elevated atop the reef platforms than in the “coral-covered plat-
555 forms” simulations, which further reflects the dissipative effect of coral cover. As wave
556 energy dissipation through shear stress is proportional to the square of the particle veloc-
557 ity (see Eq. 1), the higher velocities computed for higher-magnitude earthquake tsunamis
558 result in greater overall wave energy dissipation via bottom friction when coral cover is
559 present. This also explains why a relatively large degree of attenuation is observed for the
560 landslide-generated tsunamis, both of which produce similarly high waves (9 m and 3.5 m
561 for the landward-propagating waves, respectively). Our results show that tsunami ampli-
562 tude, which ultimately depends on the magnitude and proximity of the triggering source,
563 should also be considered when examining the buffering capacity of natural defences such
564 as coral reefs (Fig. 17).

565 While the GBR generally acts as a buffer to tsunami wave energy, despite its namesake,
566 the GBR itself does not form a continuous barrier on the mid- to outer shelf, especially
567 in the central region (Fig. 3). As a result, the buffering effect offered by coral cover varies **AQ2**
568 considerably alongshore. Turning again to the Solomon Islands earthquake scenarios
569 (Fig. 10), when coral cover is removed, the largest increases in wave amplitude and run-up
570 tend to occur landward of broad reef platforms (see also Fig. 9a, b). On the other hand,
571 areas that lie between inter-reef passages, or gaps, exhibit smaller increases in amplitude
572 and run-up. This phenomenon is consistent across source scenarios, and it is particularly
573 pronounced in cases where tsunami amplitudes are relatively high. This implies that the
574 protectiveness offered by coral cover varies alongshore because of platform placement; if
575 coral-covered platforms (particularly broad platforms) are positioned between the incom-
576 ing tsunami and the shoreline, they are more inclined to dampen the tsunami.

577 To summarise, reef cover contributes substantially to the overall buffering capacity of
578 the GBR, which is consistent with previous findings (e.g., Kunkel et al. 2006). However,
579 the GBR’s buffering capacity for any given location alongshore depends on various site-
580 specific factors, including the presence of coral cover, the relative positioning of the plat-
581 forms, and tsunami amplitude.

582 5.2 The impact of the GBR’s bathymetric-scale complexity on tsunami propagation

583 Our simulations reveal the remarkably complex ways in which tsunami waves interact with
584 the larger-scale bathymetric features (i.e., platforms, shoals, etc.) that comprise the GBR.
585 Of particular note is the platforms’ ability to focus tsunami wave energy towards shore (see
586 Fig. 8 and Online Resource 3 for the M_w 8.5 Solomon Islands earthquake simulations). In
587 a manner analogous to a convex lens focussing light, platforms cause the incoming tsu-
588 nami waves to refract inwards towards their shallower depths, inciting shoaling, positive
589 wave interference, and subsequent heightening of wave trains. Shoaling and heightening of
590 tsunami waves over shallow reefs has been observed by others, both from field-based and
591 modelling evidence (Chatenoux and Peduzzi 2005; Gelfenbaum et al. 2011). Interestingly,
592 frictional dissipation by coral cover appears to fully or partially counteract these focussing
593 effects, where waves subsequently dampen after growing in amplitude over the platforms
594 (e.g., Fig. 9). Consequently, smoothing the domain tends to enhance the platforms’ ability

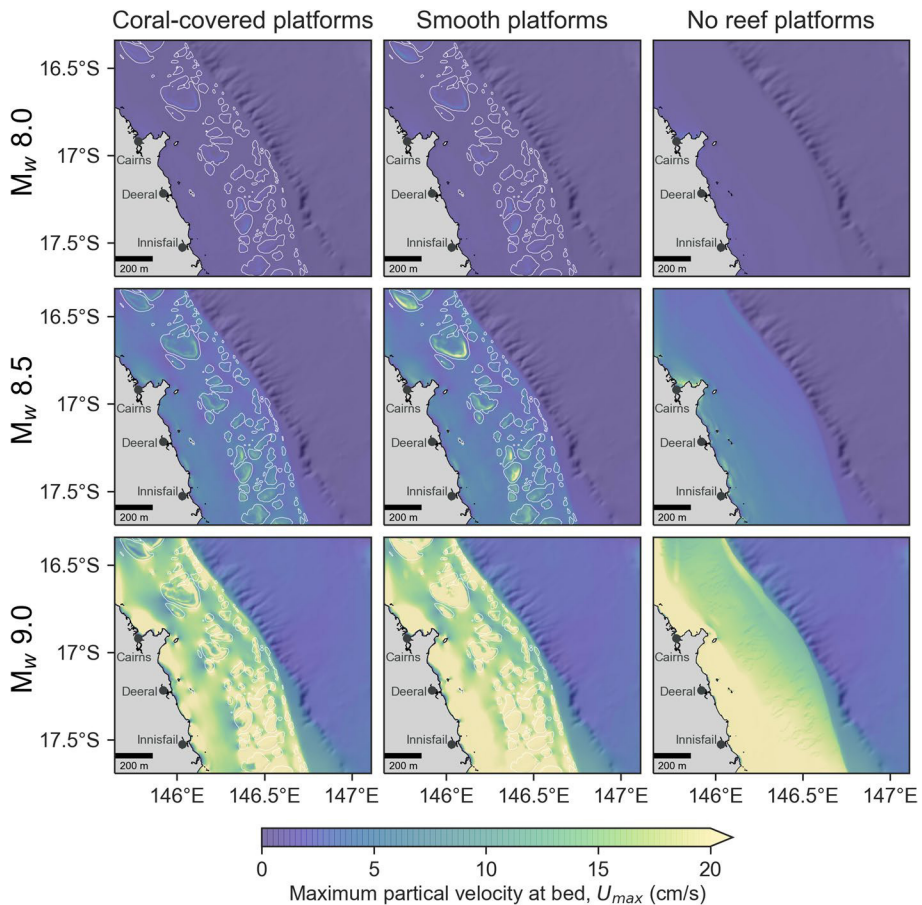


Fig. 17 Maximum bed particle velocities (in cm/s) across the computational domain for each the M_w 8.0 Solomon Islands earthquake scenario (top row), the M_w 8.5 scenario (middle row), and the M_w 9.0 scenario (bottom row). Columns are aligned based on their corresponding “coral-covered platforms” simulations (left column), “smooth platforms” simulations (middle column), and “no reef platforms” simulations (right column)

595 to focus wave energy. This is demonstrated by the higher-amplitude, landward wave trains
 596 shown in wave amplitude distributions (e.g., Fig. 9). Some platforms appear to more effective-
 597 ly focus wave energy than others, and we suspect this is due to factors such as reef
 598 morphology, size, and submergence depth. A more systematic investigation of platform
 599 characteristics warranted to test this hypothesis, particularly as coral reef cover, is expected
 600 to decline in the future.

601 In addition to focussing effects, simulated tsunamis exhibit a complex interplay of
 602 additional behaviours when interacting with platforms, such as diffraction, reflection,
 603 and scattering of wave trains (see Online Resource 5 for example). These effects are most
 604 pronounced for the landslide-generated tsunami cases (see Sect. 4.4), and we tentatively
 605 suggest that this is due to their shorter wavelengths. Our simulations further reinforce the
 606 important role that local bathymetry plays in modulating tsunami behaviour, particularly
 607 in shallow reef environments (Baba et al. 2008; Dilmen et al. 2018). This potent, complex,

608 and site-specific control on tsunami propagation further underscores the need to evaluate
609 tsunami hazard on a case-by-case basis.

610 We also highlight the intriguing role of inter-reef passages, or gaps, in modulating tsu-
611 nami behaviour as it crosses the shelf. Many have hypothesized that gaps in the reef struc-
612 ture worsen the tsunami hazard, as the gaps act as low-resistance conduits that amplify
613 wave energy (Nott 1997; Liu et al. 2005; Gelfenbaum et al. 2011; McAdoo et al. 2011;
614 Roger et al. 2014). In our simulations, porous gaps in the reef structure certainly permit
615 wave energy to pass through to the coastline. However, there is little evidence to support
616 the notion that the gaps amplify waves. In fact, due to focussing, amplification of wave
617 amplitudes occurs *over* the platforms rather than *between* them (e.g., Figs. 9, 11). In the
618 case of the GBR, many of the platforms appear to be wide enough, deep enough, far
619 enough apart, and far enough from the coastline such that the inter-reef gaps do not pose
620 a significant hazard. This is in contrast to many fringing reef systems, where gaps can be
621 quite narrow, shallow, and close to shore. We therefore suggest that for the GBR, the wave
622 focussing ability of platforms may be of greater concern for the northeastern Australian
623 coastline than the presence of gaps in the reef structure.

624 Overall, the GBR's underlying bathymetric structure contributes significantly to its
625 buffering capacity, and this becomes apparent when platforms are removed from simula-
626 tions (see Figs. 10 and 16). When platforms are removed, waves are permitted to prop-
627 agate smoothly and uninterrupted across the shelf, highlighting the highly obstructive
628 nature of the platforms themselves. Offshore wave amplitudes and run-up distributions
629 increase alongshore across all source scenarios when platforms are removed. These find-
630 ings are consistent with previous work which suggests that bathymetric irregularities on
631 the shelf exert large control on the eventual run-up distribution at the coast (Baba et al.
632 2008; Schambach et al. 2018). Even as the GBR is interrupted by gaps, the presence reef
633 structure appears to provide at least some benefit to nearly all areas of the coastline exam-
634 ined in this study.

635 5.3 Broader implications surrounding the GBR's impact on tsunami hazard

636 This study has revealed wider implications for communities situated along the northeastern
637 Australian coastline. Firstly, from a mitigation perspective, the GBR may offer greater pro-
638 tection for more severe tsunami events. In particular, the GBR may offer natural protection
639 against near-field landslide sources, which are notoriously difficult to predict and forecast
640 (Tappin et al. 1999; Harbitz et al. 2014). While this may take some pressure off warning
641 systems, we stress that coastal communities should not rely upon the GBR alone to reduce
642 their vulnerability to tsunami hazards. A holistic strategy for tsunami hazard preparedness
643 ultimately should include risk awareness, hazard education, resilient infrastructure, and
644 robust early warning systems (Baird et al. 2005; Liu et al. 2005; Dominey-Howes et al.
645 2007; Mori et al. 2011).

646 Secondly, from a *future* mitigation perspective, our work suggests that the declining
647 coral health, which is associated with globally mediated anthropogenic climate change
648 (De'ath et al. 2012; Hughes et al. 2018), will have an overall adverse effect on the GBR's
649 defensive capability. In this context, today's reef-buffering asset may be tomorrow's liabil-
650 ity. Areas of shoreline that are best-protected by broad, expansive coral-covered platforms
651 may experience the highest inundation risk in the future as coral die-off continues and as
652 architectural complexity deteriorates (Alvarez-Filip et al. 2009), enhancing the platforms'
653 ability to focus energy towards shore rather than attenuating it. These local differences

654 reinforce the need for site-specific hazard assessments when considering tsunami hazard on
655 the northeastern Australian margin in the future.

656 **5.4 Reconciling differing interpretations of coral reef impact on tsunamis**

657 In light of our results, we address some of the contrasting interpretations in the literature
658 around the impact of coral reefs on tsunami hazard. Firstly, while the GBR, being an off-
659 shore barrier system, buffers the tsunami hazard for the more distant Australian coastline,
660 other reef environments (in particular, narrow fringing reefs that surround populated inner
661 islands) could exacerbate tsunami hazard through behaviours such as shoaling, focussing,
662 and bore formation (Chatenoux and Peduzzi 2005; Fritz et al. 2011; Gelfenbaum et al.
663 2011; Yao et al. 2012). Indeed, our simulations showcase shoaling and focussing on plat-
664 forms, which locally augment wave amplitudes at the intra-platform scale. A more rigorous
665 inundation study would be needed to confirm whether this translates to increased hazard
666 within the lagoons, shoals, and islands that rest within the platforms. Therefore, coral reefs
667 could have either beneficial or detrimental effects on the overall hazard depending on the
668 type reef system in question and the proximity of coastal communities and assets to the
669 site of the most severe shoaling/focussing. In the debate surrounding reef protectiveness
670 against tsunamis, a distinction must be made between fringing reef systems and offshore
671 barrier systems, as they have different implications for proximity to wave focussing effects,
672 and therefore, exposure.

673 On the other hand, we also note potential ambiguities around the ways in which the
674 impact of coral reefs is reported in post-tsunami field surveys. From our simulations and
675 others (Kunkel et al. 2006; Uslu et al. 2010; Gelfenbaum et al. 2011), there is evidently
676 a strong theoretical basis to support the fact that coral reefs can dissipate tsunami wave
677 energy, reducing the tsunami *hazard*. However, this overall reduction in hazard may not
678 be sufficient to completely reduce the *physical vulnerability* and *exposure* of coastal com-
679 munities (Uslu et al. 2010). When discussing the buffering role of reefs, many have high-
680 lighted that despite being within close proximity to reefs, coastal assets have nonetheless
681 been destroyed during tsunami events (e.g., Baird et al. 2005), leading some to conclude
682 that coral reefs provide no protective benefit to coastal communities. In these cases, the
683 reefs could very well have buffered the overall tsunami hazard, reducing the overall inun-
684 dation and run-up extent. However, this protective benefit may not have been sufficient
685 to completely shield coastal communities that were situated close to shore. Care must be
686 taken when retrospectively interpreting the role that coral reefs may have played in reduc-
687 ing tsunami hazard along a shoreline, and a clear distinction should be made between *haz-*
688 *ard reduction* and *risk reduction*, which lies at the intersection between hazard, exposure,
689 and vulnerability.

690 **5.5 Study limitations and future work**

691 Uncertainties persist that could complicate such future tsunami hazards assessments in
692 coral reef environments. Firstly, at the ecosystem scale, the relationship between coral
693 rugosity and community composition requires more precise quantification on an intra-reef
694 platform scale (Rogers et al. 2016). This will continue to be a pressing task in the future,
695 as profound ecological shifts may be precipitated by both the immediate aftermath of the
696 tsunami impact and longer-term environmental changes, thus affecting ecosystem-scale
697 structural complexity (Madin and Connolly 2006; Alvarez-Filip et al. 2009; Ferrari et al.

698 2016; Hughes et al. 2018). While platform degradation and bioerosion is largely anti-
699 pated to flatten coral reefs (Alvarez-Filip et al. 2009), the shorter-term impact of these and
700 other stressors on ecosystem-scale rugosity is still not precisely known. These ecosystems
701 should be stringently monitored to better assess how coastal hazard severity as a whole
702 will be transformed in these areas. Additionally, the approach used to parameterize bottom
703 shear stress, though very common both in the field and in modelling studies, may need to
704 be reconfigured to account for more complex tsunami interactions and subgrid turbulent
705 dissipation within the 3D reef structure (Lowe et al. 2008; Kim et al. 2009; Rosman and
706 Hench 2011). Moreover, these more complex interactions may be better represented by a
707 Navier–Stokes model rather than a depth-averaged wave model (Kazolea et al. 2019).

708 On a larger scale, it is worth exploring the potential impact of undular bores that could
709 arise and break on the platforms themselves, as they could play an additional role in dis-
710 sipating wave energy offshore (Grilli et al. 2012; Glimsdal et al. 2013). These wave fea-
711 tures would not have been resolved in our coarser-resolution runs (Schambach et al. 2018),
712 as capturing them quickly becomes very demanding computationally (< 10 m resolution
713 required, Grilli et al. 2012). Also, while our study emphasizes the effect of the GBR on
714 offshore amplitudes and projected run-up distributions, ultimately, tsunami-induced surges
715 and bores deliver the force and high water levels that cause destruction to coastal commu-
716 nities onshore (Koshimura et al. 2009; Nistor et al. 2009; Nouri et al. 2010). Further work
717 is warranted to establish whether the reduction in offshore wave amplitude translates to a
718 reduced hazard onshore, and this would necessitate the deployment of higher-resolution
719 inundation simulations.

720 Finally, our study was not designed to provide a reappraised, comprehensive hazard
721 assessment for the northeastern Australian coastline although our findings suggest that the
722 reef's role should be considered in future assessments. That being said, we stress the need
723 for a robust parameterization of reef roughness (Nelson 1996; Rosman and Hench 2011).
724 Furthermore, as indicated by sensitivity analyses (see Online Resource 2), these propaga-
725 tion simulations require high spatial resolution (200 m for earthquake sources and 100 m
726 or less for landslide sources) in order to properly capture the reef structure and to resolve
727 complex tsunami-reef interactions. While this increases computational demand, we none-
728 theless deem it worthwhile to consider the role of the reef, as current assessments may
729 be over-estimating tsunami risk in northeast Australia. Additionally, a more meaningful
730 assessment of the submarine landslide tsunami hazard is needed to better understand the
731 timing, frequency, and magnitude of these events. In the future, it may be worth consid-
732 ering more complex failure dynamics (i.e. landslide deformation and two-way coupling
733 with the water column), which could alter the run-up results (Masson et al. 2006; Geist
734 et al. 2009; Abadie et al. 2010), but we anticipate that accounting for these dynamics will
735 not alter the overall conclusions established here about the buffering effect of the GBR.
736 Addressing these limitations will enable more reliable forecasting as the fate of the world's
737 coral reefs becomes clearer with time.

738 6 Conclusions

739 This study demonstrates the nuanced interactions between tsunamis and coral reef sys-
740 tems. In agreement with previous work we find that the Great Barrier Reef (GBR), both in
741 terms of coral cover and larger-scale bathymetric complexity, acts as a large-scale regional
742 buffer against tsunamis. However, the reef appears to provide greater protection against

743 higher-amplitude tsunamis due to the larger computed particle velocities at bed, which
744 directly dictates the degree of frictional dissipation through shear stress. Additionally, we
745 find that the protectiveness offered by the GBR locally depends on coral cover and plat-
746 form distribution. We also find that wave focussing by reef platforms could pose a greater
747 hazard than the gaps between platforms, which have been previously thought to amplify
748 waves. In the context of the larger debate about whether coral reefs reduce tsunami hazards
749 for coastal communities, we conclude that differing interpretations can be reconciled when
750 considering site-specific factors. AQ3

751 **Supplementary information** The online version contains supplementary material available at <https://doi.org/10.1007/s11069-021-04686-w>.

753 **Acknowledgements** We extend our sincere gratitude to Fengyan Shi for his assistance with model set-up
754 and troubleshooting. We also thank Lorena Moscardelli for allowing us to reproduce a significant portion
755 of her submarine landslide database for this work. We are grateful to Tristan Salles, Jon Hill, and Greg
756 Houseman for their constructive and insightful comments. Stewart Allen and Diana Greensdale from the
757 Australian Bureau of Meteorology provided earthquake source parameters. Computational resources were
758 provided by the National Computational Infrastructure (NCI) in Canberra, Australia, which is supported by
759 the Australian Commonwealth Government. We also thank the Sydney Informatics Hub at the University of
760 Sydney for the provisioning of both expertise and computing power by their high-performance computing
761 facility (Artemis).

762 **Funding** A. T. was supported by the University of Sydney DBH Scholarship, and S. B. was supported
763 through the Helmholtz Young Investigators Group CRYSTALS (VH-NG-1132).

764 **Data availability** The bathymetry of the Great Barrier Reef region can be found here: <http://eatlas.org.au/data/uuid/200aba6b-6fb6-443e-b84b-86b0bbdb53ac>. The Great Barrier Reef Banks shapefile can be
765 obtained here: <https://data.gov.au/dataset/ds-ga-c00ab093-f02d-5b03-e044-00144fdd4fa6/details?q=great%20barrier%20reef%20banks>. The global reef dataset can be downloaded here: www.wri.org/resources/datasets/reefs-risk-revisited.

769 **Code availability** The code Geowave can be downloaded here: <http://www.appliedfluids.com/geowave.html>. The codes NHWAVE and FUNWAVE-TVD can be downloaded from GitHub (github.com/JimKirby/NHWAVE; [fengyanshi.github.io/build/html/index.html](https://github.com/fengyanshi.github.io/build/html/index.html)).

772 **Declarations**

773 **Conflicts of interest** The authors have none to declare.

774 References

- 775 Abadie S, Morichon D, Grilli S, Glockner S (2010) Numerical simulation of waves generated by landslides
776 using a multiple-fluid Navier-Stokes model. *Coast Eng* 57:779–794. <https://doi.org/10.1016/j.coast>
777 [aleng.2010.03.003](https://doi.org/10.1016/j.coast)
- 778 Aksu AE, Hiscott RN (1992) Shingled quaternary debris flow lenses on the north-east Newfoundland Slope.
779 *Sedimentology* 39:193–206. <https://doi.org/10.1111/j.1365-3091.1992.tb01034.x>
- 780 Alfaro E, Holz M (2014) Seismic geomorphological analysis of deepwater gravity-driven deposits on a
781 slope system of the southern Colombian Caribbean margin. *Mar Pet Geol* 57:294–311. <https://doi.org/10.1016/j.marpetgeo.2014.06.002>
- 782 Alvarez-Filip L, Dulvy NK, Gill JA et al (2009) Flattening of Caribbean coral reefs: region-wide declines in
783 architectural complexity. *Proc R Soc B Biol Sci* 276:3019–3025. <https://doi.org/10.1098/rspb.2009.0339>
- 784 Alves TM, Cartwright JA (2009) Volume balance of a submarine landslide in the Espírito Santo Basin, off-
785 shore Brazil: quantifying seafloor erosion, sediment accumulation and depletion. *Earth Planet Sci Lett*
786 288:572–580. <https://doi.org/10.1016/j.epsl.2009.10.020>

- 789 Amante C, Eakins BW (2009) ETOPO1 Arc-Minute Global Relief Model: Procedures, Data Sources and
790 Analysis. NOAA Technical Memorandum NESDIS NGDC-24. National Geophysical Data Center,
791 NOAA
- 792 Andrews JC, Bode L (1988) The tides of the central great barrier reef. *Cont Shelf Res* 8:1057–1085. [https://doi.org/10.1016/0278-4343\(88\)90039-8](https://doi.org/10.1016/0278-4343(88)90039-8)
- 794 Ashabranner LB, Tripsanas EK, Shipp RC (2010) Multi-direction flow in a mass-transport deposit, Santos
795 Basin, offshore Brazil. In: Mosher DC, Shipp RC, Moscardelli L et al (eds) *Submarine Mass move-*
796 *ments and their consequences*. Springer, Netherlands, Dordrecht, pp 247–255
- 797 Australian Bureau of Meteorology (2020) Past Tsunami Events. <http://www.bom.gov.au/tsunami/history/index.shtml>
- 798
- 799 Baba T, Mieczko R, Burbidge D et al (2008) The effect of the great barrier reef on the propagation of the
800 2007 Solomon Islands tsunami recorded in Northeastern Australia. *Pure Appl Geophys* 165:2003–
801 2018. <https://doi.org/10.1007/s00024-008-0418-5>
- 802 Baird AH, Campbell SJ, Anggoro AW et al (2005) Acehnese reefs in the Wake of the Asian Tsunami centre
803 for coral reef biodiversity. *Curr Biol* 15:1926–1930. <https://doi.org/10.1016/j.cub.2005.09.036>
- 804 Barnes PM, Lewis KB (1991) Sheet slides and rotational failures on a convergent margin: the Kidnappers
805 Slide, New Zealand. *Sedimentology* 38:205–221. <https://doi.org/10.1111/j.1365-3091.1991.tb01257.x>
- 806
- 807 Beaman RJ (2010) Project 3D-GBR: a high-resolution depth model for the great barrier reef and Coral Sea.
808 Project 2.5i.1a Final Report, Marine and Tropical Sciences Research Facility, Cairns, Australia
- 809 Behrmann JH, Völker D, Geersen J et al (2014) Size-frequency relationship of submarine landslides at
810 convergent plate margins: implications for hazard and risk assessment. In: Krastel S, Behrmann J-H,
811 Völker D et al (eds) *Submarine mass movements and Their consequences: 6th International Sympos-*
812 *ium*. Springer International Publishing, Cham, pp 165–175
- 813 Bellwood DR, Hughes TP, Folke C, Nyström M (2004) Confronting the coral reef crisis. *Nature* 429:827–
814 833. <https://doi.org/10.1038/nature02691>
- 815 Boudon G, Le Friant A, Komorowski J et al (2007) Volcano flank instability in the lesser antilles arc: diversity
816 of scale, processes, and temporal recurrence. *J Geophys Res Solid Earth* 112:B08205. <https://doi.org/10.1029/2006JB004674>
- 817
- 818 Bourget J, Zaragosi S, Ellouz-Zimmermann N et al (2011) Turbidite system architecture and sedimentary
819 processes along topographically complex slopes: the Makran convergent margin. *Sedimentology*
820 58:376–406. <https://doi.org/10.1111/j.1365-3091.2010.01168.x>
- 821 Bourget J, Zaragosi S, Rodriguez M et al (2013) Late Quaternary megaturbidites of the Indus fan: origin and
822 stratigraphic significance. *Mar Geol* 336:10–23. <https://doi.org/10.1016/j.margeo.2012.11.011>
- 823 Boyd R, Keene J, Hubble T, et al (2010) Southeast Australia: a Cenozoic continental margin dominated by
824 mass transport. In: *Submarine mass movements and their consequences*. pp 491–502
- 825 Bozec Y-M, Alvarez-Filip L, Mumby PJ (2015) The dynamics of architectural complexity on coral reefs
826 under climate change. *Glob Chang Biol* 21:223–235. <https://doi.org/10.1111/gcb.12698>
- 827 Brune S, Babeyko a. Y, Ladage S, Sobolev S V. (2010) Landslide tsunami hazard in the Indonesian Sunda
828 Arc. *Nat Hazards Earth Syst Sci* 10:589–604. 10.5194/nhess-10-589-2010
- 829 Burke L, Reyter K, Spalding M, Perry A (2011) Reefs at risk revisited. World Resources Institute, Washing-
830 ton, DC
- 831 Calvès G, Huuse M, Clift PD, Brusset S (2015) Giant fossil mass wasting off the coast of West India: the
832 Nataraja submarine slide. *Earth Planet Sci Lett* 432:265–272. <https://doi.org/10.1016/j.epsl.2015.10.022>
- 833
- 834 Camerlenghi A, Accettella D, Costa S et al (2009) Morphogenesis of the SW Balearic continental slope and
835 adjacent abyssal plain, Western Mediterranean Sea. *Int J Earth Sci* 98:735. <https://doi.org/10.1007/s00531-008-0354-8>
- 836
- 837 Campbell DC, Mosher DC (2010) Middle to Late Miocene Slope Failure and the Generation of a Regional
838 Unconformity Beneath the Western Scotian Slope, Eastern Canada BT - Submarine Mass Movements
839 and Their Consequences. In: Mosher DC, Shipp RC, Moscardelli L, et al. (eds). Springer Nether-
840 lands, Dordrecht, pp 645–655
- 841 Canals M, Lastras G, Urgeles R et al (2004) Slope failure dynamics and impacts from seafloor and shallow
842 sub-seafloor geophysical data: case studies from the COSTA project. *Mar Geol* 213:9–72. <https://doi.org/10.1016/j.margeo.2004.10.001>
- 843
- 844 Carlson PR, Karl HA, Edwards BD, et al (1993) Mass movement related to large submarine canyons along
845 the Beringian Margin, Alaska. In: *Submarine Landslides: Selected Studies in the US Exclusive Eco-*
846 *nomic Zone*. U.S. Geological Survey Bulletin, Washington, DC, p 104
- 847 Center for International Earth Science Information Network (CIESIN) (2018) Gridded Population of the
848 World, Version 4 (GPWv4): Population Density Adjusted to Match 2015 Revision UN WPP Country

- 849 Totals, Revision 11. NASA Socioeconomic Data and Applications Center (SEDAC), Columbia Uni-
850 versity, Palisades, NY
- 851 Chatenoux B, Peduzzi P (2005) Analysis on the role of bathymetry and other environmental parameters in
852 the impacts from the 2004 Indian Ocean Tsunami. UNEP/GRID-Europe, Geneva
- 853 Chatenoux B, Peduzzi P (2007) Impacts from the 2004 Indian Ocean tsunami: analysing the poten-
854 tial protecting role of environmental features. *Nat Hazards* 40:289–304. [https://doi.org/10.1007/](https://doi.org/10.1007/s11069-006-0015-9)
855 [s11069-006-0015-9](https://doi.org/10.1007/s11069-006-0015-9)
- 856 Chaytor JD, ten Brink US, Solow AR, Andrews BD (2009) Size distribution of submarine landslides along
857 the U.S. Atlantic margin *Mar Geol* 264:16–27. <https://doi.org/10.1016/j.margeo.2008.08.007>
- 858 Chaytor JD, Twichell DC, Lynett P, Geist EL (2010) Distribution and Tsunamiogenic Potential of submarine
859 landslides in the Gulf of Mexico. In: Mosher DC, Shipp RC, Moscardelli L et al (eds) *Submarine*
860 *mass movements and their consequences*. Springer, Netherlands, Dordrecht, pp 745–754
- 861 Chaytor JD, Twichell DC, ten Brink US (2012) A reevaluation of the Munson-Nygren-retriever subma-
862 rine landslide complex, Georges bank lower slope, Western North Atlantic. In: Yamada Y, Kawamura
863 K, Ikehara K et al (eds) *Submarine mass movements and their consequences*. Springer, Netherlands,
864 Dordrecht, pp 135–146
- 865 Chaytor JD, Geist EL, Paull CK et al (2016) Source characterization and tsunami modeling of submarine
866 landslides along the Yucatán Shelf/Campeche Escarpment, Southern Gulf of Mexico. *Pure Appl Geophy*
867 *s* 173:4101–4116. <https://doi.org/10.1007/s00024-016-1363-3>
- 868 Collot J, Lewis K, Lamarche G, Lallemand S (2001) The giant Ruatoria debris avalanche on the northern
869 Hikurangi margin, New Zealand: result of oblique seamount subduction. *J Geophys Res Solid Earth*
870 106:19271–19297. <https://doi.org/10.1029/2001JB900004>
- 871 Dalla Valle G, Gamberi F, Foglini F, Trincardi F (2015) The Gondola slide: a mass transport complex
872 controlled by margin topography (South-Western Adriatic Margin, Mediterranean Sea). *Mar Geol*
873 366:97–113. <https://doi.org/10.1016/j.margeo.2015.05.001>
- 874 Davies G, Griffin J (2018) The 2018 Australian probabilistic Tsunami hazard assessment: hazard from
875 earthquake generated Tsunamis. *Geoscience Australia, Canberra*
- 876 Davies PJ, McKenzie JA, Palmer-Julson AA, et al (1991) Site 819. In: McKenzie JA, Palmer-Julson AA,
877 Betzler C, et al. (eds) *Proceedings of the Ocean Drilling Program, Part A: Initial Reports*. College
878 Station: TX (Ocean Drilling Program), p 451
- 879 de Lalouvière C la H, Gracia V, Sierra JP, et al (2020) Impact of Climate Change on Nearshore Waves at a
880 Beach Protected by a Barrier Reef. *Water* 12:1681
- 881 De'ath G, Fabricius KE, Sweatman H, Puotinen M, (2012) The 27-year decline of coral cover on the great
882 barrier reef and its causes. *Proc Natl Acad Sci U S A* 109:17995–17999. [https://doi.org/10.1073/pnas.](https://doi.org/10.1073/pnas.1208909109)
883 [1208909109](https://doi.org/10.1073/pnas.1208909109)
- 884 Dillon WP, Risch JS, Scanlon KM et al (1993) Ancient crustal fractures control the location and size of
885 collapsed blocks at the Blake Escarpment, east of Florida. In: Lee H, Twichell D (eds) *Schwab W.*
886 *Submarine landslides, Selected Studies in the US Exclusive Economic Zone*. US Geological Survey
887 *Bulletin*, pp 54–59
- 888 Dilmen DI, Roe GH, Wei Y, Titov VV (2018) The role of near-shore Bathymetry during Tsunami Inun-
889 dation in a Reef Island setting: a case study of Tutuila Island. *Pure Appl Geophys* 175:1239–1256.
890 <https://doi.org/10.1007/s00024-018-1769-1>
- 891 Dingle RV (1977) The anatomy of a large submarine slump on a sheared continental margin (SE Africa). *J*
892 *Geol Soc London* 134:293–310. <https://doi.org/10.1144/gsjgs.134.3.0293>
- 893 Dingle RV (1980) Large allochthonous sediment masses and their role in the construction of the continental
894 slope and rise off southwestern Africa. *Mar Geol* 37:333–354. [https://doi.org/10.1016/0025-3227\(80\)](https://doi.org/10.1016/0025-3227(80)90109-7)
895 [90109-7](https://doi.org/10.1016/0025-3227(80)90109-7)
- 896 Dominey-Howes D (2007) Geological and historical records of tsunamis in Australia. *Mar Geol* 239:99–123.
897 <https://doi.org/10.1016/j.margeo.2007.01.010>
- 898 Dominey-Howes D, Papathoma-Köhle M, Bird D et al (2007) Letter to the editor: the Australian Tsunami
899 warning system and lessons from the 2 April 2007 Solomon Islands tsunami alert in Australia. *Nat*
900 *Hazards Earth Syst Sci* 7:571–572
- 901 Droz L, Dos Reis AT, Rabineau M et al (2006) Quaternary turbidite systems on the northern margins of the
902 Balearic Basin (Western Mediterranean): a synthesis. *Geo-Marine Lett* 26:347–359
- 903 Eichhubl P, Greene HG, Maher N (2002) Physiography of an active transpressive margin basin: high-reso-
904 lution bathymetry of the Santa Barbara basin, Southern California continental borderland. *Mar Geol*
905 184:95–120. [https://doi.org/10.1016/S0025-3227\(01\)00280-8](https://doi.org/10.1016/S0025-3227(01)00280-8)
- 906 Elger J, Berndt C, Krastel S et al (2015) The fram slide off Svalbard: a submarine landslide on a low-sedi-
907 mentation-rate glacial continental margin. *J Geol Soc London* 172:153–156. [https://doi.org/10.1144/](https://doi.org/10.1144/jgs2014-055)
908 [jgs2014-055](https://doi.org/10.1144/jgs2014-055)

- 909 Elmore RD, Pilkey OH, Clearly WJ, Curran HA (1979) Black Shell turbidite, Hatteras Abyssal plain, western Atlantic Ocean. *Geol Soc Am Bull* 90:1165–1176. [https://doi.org/10.1130/0016-7606\(1979\)90%3c1165:BSTHAP%3e2.0.CO;2](https://doi.org/10.1130/0016-7606(1979)90%3c1165:BSTHAP%3e2.0.CO;2)
- 910
- 911
- 912 Elverhøi A, de Blasio FV, Butt FA et al (2002) Submarine mass-wasting on glacially-influenced continental slopes: processes and dynamics. *Geol Soc London Spec Publ* 203:73–87. <https://doi.org/10.1144/GSL.SP.2002.203.01.05>
- 913
- 914
- 915 Embley RW (1982) Anatomy of some Atlantic margin sediment slides and some comments on ages and mechanisms. In: *Marine slides and other mass movements*. Springer, pp 189–213
- 916
- 917 Enet F, Grilli ST (2007) Experimental study of tsunami generation by three-dimensional rigid underwater landslides. *J Waterw Port Coastal Ocean Eng* 133:442–454. [https://doi.org/10.1061/\(ASCE\)0733-950X\(2007\)133:6\(442\)](https://doi.org/10.1061/(ASCE)0733-950X(2007)133:6(442))
- 918
- 919
- 920 Fernando HJS, McCulley JL, Mendis SG, Perera K (2005) Coral poaching worsens tsunami destruction in Sri Lanka. *Eos Trans Am Geophys Union* 86:301–304. <https://doi.org/10.1029/2005EO330002>
- 921
- 922 Ferrari R, Bryson M, Bridge T et al (2016) Quantifying the response of structural complexity and community composition to environmental change in marine communities. *Glob Chang Biol* 22:1965–1975. <https://doi.org/10.1111/gcb.13197>
- 923
- 924
- 925 Ferrario F, Beck MW, Storlazzi CD et al (2014) The effectiveness of coral reefs for coastal hazard risk reduction and adaptation. *Nat Commun* 5:3794. <https://doi.org/10.1038/ncomms4794>
- 926
- 927 Fine IV, Rabinovich AB, Bornhold BD et al (2005) The grand banks landslide-generated tsunami of November 18, 1929: preliminary analysis and numerical modeling. *Mar Geol* 215:45–57. <https://doi.org/10.1016/j.margeo.2004.11.007>
- 928
- 929
- 930 Ford M, Becker JM, Merrifield MA, Song YT (2014) Marshall Islands fringing reef and Atoll Lagoon observations of the Tohoku Tsunami. *Pure Appl Geophys* 171:3351–3363. <https://doi.org/10.1007/s00024-013-0757-8>
- 931
- 932
- 933 Freire F, Gyllencreutz R, Jafri RU, Jakobsson M (2014) Acoustic evidence of a submarine slide in the deepest part of the Arctic, the Molloy Hole. *Geo-Marine Lett* 34:315–325
- 934
- 935 Frey-Martínez J, Cartwright J, James D (2006) Frontally confined versus frontally emergent submarine landslides: a 3D seismic characterisation. *Mar Pet Geol* 23:585–604. <https://doi.org/10.1016/j.marpetgeo.2006.04.002>
- 936
- 937
- 938 Fritz HM, Borrero JC, Synolakis CE et al (2011) Insights on the 2009 South Pacific tsunami in Samoa and Tonga from field surveys and numerical simulations. *Earth-Sci Rev* 107:66–75. <https://doi.org/10.1016/j.earscirev.2011.03.004>
- 939
- 940
- 941 Fryer GJ, Watts P, Pratson LF (2004) Source of the great tsunami of 1 april 1946: a landslide in the upper Aleutian forearc. *Mar Geol* 203:201–218. [https://doi.org/10.1016/S0025-3227\(03\)00305-0](https://doi.org/10.1016/S0025-3227(03)00305-0)
- 942
- 943 Fujii Y, Satake K, Sakai S et al (2011) Tsunami source of the 2011 off the Pacific coast of Tohoku Earthquake. *Earth Planets Sp* 63:55. <https://doi.org/10.5047/eps.2011.06.010>
- 944
- 945 Gallop SL, Young IR, Ranasinghe R et al (2014) The large-scale influence of the great barrier reef matrix on wave attenuation. *Coral Reefs* 33:1167–1178. <https://doi.org/10.1007/s00338-014-1205-7>
- 946
- 947 Gamberi F, Rovere M, Marani M (2011) Mass-transport complex evolution in a tectonically active margin (Gioia Basin, Southeastern Tyrrhenian Sea). *Mar Geol* 279:98–110. <https://doi.org/10.1016/j.margeo.2010.10.015>
- 948
- 949
- 950 Gardner JV, Prior DB, Field ME (1999) Humboldt slide—a large shear-dominated retrogressive slope failure. *Mar Geol* 154:323–338. [https://doi.org/10.1016/S0025-3227\(98\)00121-2](https://doi.org/10.1016/S0025-3227(98)00121-2)
- 951
- 952 Garziglia S, Sultan N, Cattaneo A et al (2010) Identification of Shear Zones and their causal mechanisms using a combination of cone penetration tests and seismic data in the eastern Niger Delta. In: Mosher DC, Shipp RC, Moscardelli L et al (eds) *Submarine mass movements and their consequences*. Springer, Netherlands, Dordrecht, pp 55–65
- 953
- 954
- 955
- 956 Gaullier V, Loncke L, Droz L et al. (2010) Slope instability on the French Guiana transform margin from swath-bathymetry and 3.5 kHz echograms. In: *Submarine Mass Movements and Their Consequences*. Springer, pp 569–579
- 957
- 958
- 959 Gee MJR, Gawthorpe RL, Friedmann SJ (2006) Triggering and evolution of a giant submarine landslide, offshore Angola, revealed by 3D seismic stratigraphy and geomorphology. *J Sediment Res* 76:9–19. <https://doi.org/10.2110/jsr.2006.02>
- 960
- 961
- 962 Gee MJR, Uy HS, Warren J et al (2007) The Brunei slide: a giant submarine landslide on the North West Borneo Margin revealed by 3D seismic data. *Mar Geol* 246:9–23. <https://doi.org/10.1016/j.margeo.2007.07.009>
- 963
- 964
- 965 Geersen J, Völker D, Behrmann JH et al (2011) Pleistocene giant slope failures offshore Arauco peninsula, southern Chile. *J Geol Soc London* 168:1237–1248. <https://doi.org/10.1144/0016-76492011-027>
- 966
- 967 Geist EL, Lynett PJ, Chaytor JD (2009) Hydrodynamic modeling of tsunamis from the Currituck landslide. *Mar Geol* 264:41–52. <https://doi.org/10.1016/j.margeo.2008.09.005>
- 968

- 969 Gelfenbaum G, Apotos A, Stevens AW, Jaffe B (2011) Effects of fringing reefs on tsunami inundation:
970 American Samoa. *Earth Sci Rev* 107:12–22. <https://doi.org/10.1016/j.earscirev.2010.12.005>
- 971 Georgiopolou A, Masson DG, Wynn RB, Krastel S (2010) Sahara Slide: age, initiation, and processes
972 of a giant submarine slide. *Geochem Geophys Geosyst* . <https://doi.org/10.1029/2010GC003066>
- 973 Giles MK, Mosher DC, Piper DJW, Wach GD (2010) Mass transport deposits on the southwestern New-
974 foundland Slope. In: *Submarine Mass Movements and Their Consequences*. Springer, pp 657–665
- 975 Glimsdal S, Pedersen GK, Harbitz CB, Løvholt F (2013) Dispersion of tsunamis: does it really matter?
976 *Nat Hazards Earth Syst Sci* 13:1507–1526. <https://doi.org/10.5194/nhess-13-1507-2013>
- 977 Goldfinger C, Kulm LD, McNeill LC, Watts P (2000) Super-scale failure of the southern Oregon Casca-
978 dia margin. *Pure Appl Geophys* 157:1189–1226. <https://doi.org/10.1007/s000240050023>
- 979 Graham NAJ, Nash KL (2013) The importance of structural complexity in coral reef ecosystems. *Coral*
980 *Reefs* 32:315–326. <https://doi.org/10.1007/s00338-012-0984-y>
- 981 Grantz A, Phillips RL, Mullen MW et al (1996) Character, paleoenvironment, rate of accumulation, and
982 evidence for seismic triggering of Holocene turbidites, Canada Abyssal Plain, Arctic Ocean. *Mar*
983 *Geol* 133:51–73. [https://doi.org/10.1016/0025-3227\(96\)00015-1](https://doi.org/10.1016/0025-3227(96)00015-1)
- 984 Greenslade DJM, Simanjuntak MA, Allen SCR (2009) An enhanced tsunami scenario database: T2.
985 Center for Australian Weather and Climate Research (CAWCR) Technical Report No. 014
- 986 Grilli ST, Harris JC, Shi F et al (2012) Numerical modeling of coastal tsunami impact dissipation and
987 impact. *Coast Eng Proc* 1:1–12
- 988 Grilli ST, O'Reilly C, Harris JC et al (2015) Modeling of SMF tsunami hazard along the upper US East
989 Coast: detailed impact around Ocean City, MD. *Nat Hazards* 76:705–746. <https://doi.org/10.1007/s11069-014-1522-8>
- 990
- 991 Grindlay N (1998) Volume and density approximations of material involved in a debris avalanche on the
992 South Slope of the Puerto Rico Trench: a report to the Puerto Rico Civil Defense and the Univer-
993 sity of Puerto Rico Sea Grant College Program. Univ North Carolina Wilmington
- 994 Haffidason H, Lien R, Sejrup HP et al (2005) The dating and morphometry of the Storegga Slide. *Mar*
995 *Pet Geol* 22:123–136. <https://doi.org/10.1016/j.marpetgeo.2004.10.008>
- 996 Hampton MA, Lee HJ, Locat J (1996) Submarine landslides. *Rev Geophys* 34:33–59. <https://doi.org/10.1029/95RG03287>
- 997
- 998 Harbitz CB, Løvholt F, Bungum H (2014) Submarine landslide tsunamis: how extreme and how likely?
999 *Nat Hazards* 72:1341–1374. <https://doi.org/10.1007/s11069-013-0681-3>
- 1000 Harders R, Ranero CR, Weinrebe W, Behrmann JH (2011) Submarine slope failures along the conver-
1001 gent continental margin of the Middle America Trench. *Geochem Geophys Geosyst* 12:n/a-n/a.
1002 <https://doi.org/10.1029/2010GC003401>
- 1003 Harris DL, Rovere A, Casella E et al. (2018) Coral reef structural complexity provides important coastal
1004 protection from waves under rising sea levels. *Sci Adv* 4:eaa04350. <https://doi.org/10.1126/sciadv.aao4350>
- 1005
- 1006 Hengesh JV, Dirstein JK, Stanley AJ (2013) Landslide geomorphology along the Exmouth plateau conti-
1007 nental margin, North West Shelf, Australia. *Aust Geomech* 48:71–92
- 1008 Henrich R, Hanebuth TJJ, Krastel S et al (2008) Architecture and sediment dynamics of the Mauritania
1009 slide complex. *Mar Pet Geol* 25:17–33. <https://doi.org/10.1016/j.marpetgeo.2007.05.008>
- 1010 Hieke W, Werner F (2000) The Augias megaturbidite in the central Ionian Sea (central Mediterranean)
1011 and its relation to the Holocene Santorini event. *Sediment Geol* 135:205–218. [https://doi.org/10.1016/S0037-0738\(00\)00072-5](https://doi.org/10.1016/S0037-0738(00)00072-5)
- 1012
- 1013 Hine AC, Locker SD, Tedesco LP et al (1992) Megabreccia shedding from modern, low-relief carbon-
1014 ate platforms, Nicaraguan Rise. *GSA Bull* 104:928–943. [https://doi.org/10.1130/0016-7606\(1992\)104%3c0928:MSFMLR%3e2.3.CO;2](https://doi.org/10.1130/0016-7606(1992)104%3c0928:MSFMLR%3e2.3.CO;2)
- 1015
- 1016 Hinestroza G, Webster JM, Beaman RJ (2016) Postglacial sediment deposition along a mixed carbonate-
1017 siliciclastic margin: new constraints from the drowned shelf-edge reefs of the great barrier reef,
1018 Australia. *Palaeogeogr Palaeoclimatol Palaeoecol* 446:168–185. <https://doi.org/10.1016/j.palaeo.2016.01.023>
- 1019
- 1020 Hjelstuen BO, Eldholm O, Faleide JJ (2007) Recurrent Pleistocene mega-failures on the SW Barents sea
1021 margin. *Earth Planet Sci Lett* 258:605–618. <https://doi.org/10.1016/j.epsl.2007.04.025>
- 1022 Holcomb RT, Searle RC (1991) Large landslides from oceanic volcanoes. *Mar Georesour Geotechnol*
1023 10:19–32. <https://doi.org/10.1080/10641199109379880>
- 1024 Holmes R, Long D, Dodd LR (1998) Large-scale debrites and submarine landslides on the Barra Fan,
1025 west of Britain. *Geol Soc London Spec Publ* 129:67–79. <https://doi.org/10.1144/GSL.SP.1998.129.01.05>
- 1026
- 1027 Hopley D, Smithers SG, Parnell K (2007) *The geomorphology of the great barrier reef: development,*
1028 *diversity and change*. Cambridge University Press, Cambridge

- 1029 Horozal S, Bahk JJ, Lee SH et al (2016) Late Neogene-Quaternary submarine mass wasting along the
1030 margins of the Ulleung Basin, East Sea: geomorphologic controls and geohazard potential. *Quat Int*
1031 392:69–98. <https://doi.org/10.1016/j.quaint.2015.06.056>
- 1032 Horrillo J, Wood A, Kim G, Parambath A (2013) A simplified 3-D Navier-Stokes numerical model for land-
1033 slide-tsunami: application to the Gulf of Mexico. *J Geophys Res Ocean* 118:6934–6950. <https://doi.org/10.1002/2012JC008689>
- 1034 Hubble T, Webster J, Yu P et al (2016) Submarine landslides and incised canyons of the Southeast Queens-
1035 land continental margin. In: Lamarche G, Mountjoy J, Bull S et al (eds) *Submarine Mass Movements*
1036 *and their Consequences: 7th International Symposium*. Springer International Publishing, Cham, pp
1037 125–134
- 1038 Hughes TP, Kerry JT, Baird AH et al (2018) Global warming transforms coral reef assemblages. *Nature*
1039 556:492–496. <https://doi.org/10.1038/s41586-018-0041-2>
- 1040 Hühnerbach V, Masson DG, Bohrmann G et al (2005) Deformation and submarine landsliding caused by
1041 seamount subduction beneath the Costa Rica continental margin — new insights from high-resolution
1042 sidescan sonar data. *Geol Soc London Spec Publ* 244:195–205. [https://doi.org/10.1144/GSL.SP.2005.](https://doi.org/10.1144/GSL.SP.2005.244.01.12)
1043 [244.01.12](https://doi.org/10.1144/GSL.SP.2005.244.01.12)
- 1044 Hunt JE (2012) Determining the provenance, recurrence, magnitudes and failure mechanisms of submarine
1045 landslides from the Moroccan margin and Canary Islands using distal turbidite records. University of
1046 Southampton
- 1047 Hunt JE, Wynn RB, Talling PJ, Masson DG (2013) Frequency and timing of landslide-triggered turbidity
1048 currents within the Agadir Basin, offshore NW Africa: are there associations with climate change, sea
1049 level change and slope sedimentation rates? *Mar Geol* 346:274–291. [https://doi.org/10.1016/j.margeo.](https://doi.org/10.1016/j.margeo.2013.09.004)
1050 [2013.09.004](https://doi.org/10.1016/j.margeo.2013.09.004)
- 1051 Kazolea M, Filippini A, Ricchiuto M et al (2019) Wave propagation, breaking, and overtopping on a 2D
1052 reef: a comparative evaluation of numerical codes for tsunami modelling. *Eur J Mech - B/Fluids*
1053 73:122–131. <https://doi.org/10.1016/j.euromechflu.2017.10.010>
- 1054 Kim D-H, Lynett PJ, Socolofsky SA (2009) A depth-integrated model for weakly dispersive, turbulent, and
1055 rotational fluid flows. *Ocean Model* 27:198–214. <https://doi.org/10.1016/j.ocemod.2009.01.005>
- 1056 Koshimura S, Namegaya Y, Yanagisawa H (2009) Tsunami fragility: a new measure to identify tsunami
1057 damage. *J Disaster Res* 4:479–488. <https://doi.org/10.20965/jdr.2009.p0479>
- 1058 Kowalik Z, Knight W, Logan T, Whitmore P (2005) Numerical modeling of the global tsunami: Indonesian
1059 tsunami of 26 December 2004. *Sci Tsunami Hazards* 23:40–56
- 1060 Krastel S, Wynn RB, Georgiopolou A et al (2012) Large-scale mass wasting on the Northwest African
1061 continental margin: some general implications for mass wasting on passive continental margins. In:
1062 Yamada Y, Kawamura K, Ikehara K et al (eds) *Submarine mass movements and their consequences*.
1063 Springer, Netherlands, Dordrecht, pp 189–199
- 1064 Kunkel CM, Hallberg RW, Oppenheimer M (2006) Coral reefs reduce tsunami impact in model simulations.
1065 *Geophys Res Lett* 33:L23612. <https://doi.org/10.1029/2006GL027892>
- 1066 Kvalstad TJ, Gauer P, Kayina AM, et al. (2002) Slope stability at Ormen Lange: Offshore site investigation
1067 and geotechnics. In: *Diversity and Sustainability, Proceedings of an International Conference*, Lon-
1068 don. pp 233–250
- 1069 Laberg JS, Kawamura K, Amundsen H et al (2014) A submarine landslide complex affecting the Jan Mayen
1070 Ridge, Norwegian-Greenland sea: slide-scar morphology and processes of sediment evacuation. *Geo-*
1071 *Marine Lett* 34:51–58
- 1072 Lallemand S, Lehu R, Rétif F et al (2015) A ~3000 years-old sequence of extreme events revealed by
1073 marine and shore deposits east of Taiwan. *Tectonophysics* 692:325–341. [https://doi.org/10.1016/j.](https://doi.org/10.1016/j.tecto.2015.11.001)
1074 [tecto.2015.11.001](https://doi.org/10.1016/j.tecto.2015.11.001)
- 1075 Lamarche G, Joanne C, Collot J (2008) Successive, large mass-transport deposits in the south Kermadec
1076 fore-arc basin, New Zealand: the Matakaoa submarine instability complex. *Geochem Geophys Geos-*
1077 *yst*. <https://doi.org/10.1029/2007GC001843>
- 1078 Lastras G, De Blasio FV, Canals M, Elverhøi A (2005) Conceptual and numerical modeling of the BIG'95
1079 debris flow, western Mediterranean Sea. *J Sediment Res* 75:784–797. [https://doi.org/10.2110/jsr.](https://doi.org/10.2110/jsr.2005.063)
1080 [2005.063](https://doi.org/10.2110/jsr.2005.063)
- 1081 Lastras G, Canals M, Urgeles R et al (2007) A walk down the cap de Creus canyon, Northwestern Mediter-
1082 ranean sea: Recent processes inferred from morphology and sediment bedforms. *Mar Geol* 246:176–
1083 192. <https://doi.org/10.1016/j.margeo.2007.09.002>
- 1084 Le Friant A, Ishizuka O, Boudon G et al (2015) Submarine record of volcanic island construction and col-
1085 lapse in the lesser antilles arc: first scientific drilling of submarine volcanic island landslides by IOD-
1086 PExpedition 340. *Geochemistry, Geophys Geosystems* 16:420–442. [https://doi.org/10.1002/2014G](https://doi.org/10.1002/2014GC005652)
1087 [C005652](https://doi.org/10.1002/2014GC005652)
- 1088

- 1089 Lebas E, Le Friant A, Boudon G et al (2011) Multiple widespread landslides during the long-term evolution
1090 of a volcanic island: insights from high-resolution seismic data, Montserrat, Lesser Antilles. *Geo-*
1091 *chem Geophys Geosyst* 12:Q05006. <https://doi.org/10.1029/2010GC003451>
- 1092 Lebreiro SM, McCave IN, Weaver PPE (1997) Late Quaternary turbidite emplacement on the Horseshoe
1093 abyssal plain (Iberian margin). *J Sediment Res Sect A Sediment Petrol Process* 67:856–870
- 1094 Lee HJ (2009) Timing of occurrence of large submarine landslides on the Atlantic Ocean margin. *Mar Geol*
1095 264:53–64. <https://doi.org/10.1016/j.margeo.2008.09.009>
- 1096 Lee C, Nott JA, Keller FB, Parrish AR (2004) Seismic expression of the Cenozoic mass transport com-
1097 plexes, deepwater Tarfaya-Agadir Basin, offshore Morocco. In: *Offshore Technology Conference*.
1098 *Offshore Technology Conference*, Houston, Texas, p OTC-16741-MS
- 1099 Lee HJ, Normark WR, Fisher MA, et al. (2004) Timing and extent of submarine landslides in Southern
1100 California. In: *Offshore Technology Conference*. *Offshore Technology Conference*, Houston, Texas,
1101 p OTC-16744-MS
- 1102 Leslie SC, Mann P (2016) Giant submarine landslides on the Colombian margin and tsunami risk in the
1103 Caribbean Sea. *Earth Planet Sci Lett* 449:382–394. <https://doi.org/10.1016/j.epsl.2016.05.040>
- 1104 Li L, Switzer AD, Wang Y et al (2015) What caused the mysterious eighteenth century tsunami that struck
1105 the southwest Taiwan coast? *Geophys Res Lett* 42:8498–8506. <https://doi.org/10.1002/2015GL065567>
- 1106
- 1107 Li L, Switzer AD, Wang Y et al. (2018) A modest 0.5-m rise in sea level will double the tsunami hazard in
1108 Macau. *Sci Adv* 4:eaat1180. <https://doi.org/10.1126/sciadv.aat1180>
- 1109 Lindberg B, Laberg JS, Vorren TO (2004) The Nyk Slide—morphology, progression, and age of a partly
1110 buried submarine slide offshore northern Norway. *Mar Geol* 213:277–289. <https://doi.org/10.1016/j.margeo.2004.10.010>
- 1111
- 1112 Liu PLF, Lynett P, Fernando H et al (2005) Observations by the international tsunami survey team in Sri
1113 Lanka. *Science* 308:1595. <https://doi.org/10.1126/science.1110730>
- 1114 Lo IC, Gràcia E, Zaniboni F et al (2012) Large, deepwater slope failures: implications for landslide-gener-
1115 ated tsunamis. *Geology* 40:931–934. <https://doi.org/10.1130/G33446.1>
- 1116 Locat J, Lee H, Uri S et al (2009) Geomorphology, stability and mobility of the Currituck slide. *Mar Geol*
1117 264:28–40. <https://doi.org/10.1016/j.margeo.2008.12.005>
- 1118 Locat J, ten Brink US, Chaytor JD (2010) The block composite submarine landslide, Southern New England
1119 Slope, U.S.A.: a morphological analysis. In: Mosher DC, Shipp RC, Moscardelli L et al (eds) *Subma-*
1120 *rine mass movements and their consequences*. Springer, Netherlands, Dordrecht, pp 267–277
- 1121 Longpré M-A, Chadwick JP, Wijbrans J, Iping R (2011) Age of the El Golfo debris avalanche, El Hierro
1122 (Canary Islands): new constraints from laser and furnace $^{40}\text{Ar}/^{39}\text{Ar}$ dating. *J Volcanol Geotherm Res*
1123 203:76–80. <https://doi.org/10.1016/j.jvolgeores.2011.04.002>
- 1124 Lowe RJ, Shavit U, Falter JL et al (2008) Modeling flow in coral communities with and without waves: a
1125 synthesis of porous media and canopy flow approaches. *Limnol Oceanogr* 53:1595. <https://doi.org/10.4319/lo.2008.53.6.2668>
- 1126
- 1127 Ma G, Kirby JT, Shi F (2013) Numerical simulation of tsunami waves generated by deformable submarine
1128 landslides. *Ocean Model* 69:146–165. <https://doi.org/10.1016/j.ocemod.2013.07.001>
- 1129 Madin JS, Connolly SR (2006) Ecological consequences of major hydrodynamic disturbances on coral
1130 reefs. *Nature* 444:477–480. <https://doi.org/10.1038/nature05328>
- 1131 Maslin M, Vilela C, Mikkelsen N, Grootes P (2005) Causes of catastrophic sediment failures of the Amazon
1132 Fan. *Quat Sci Rev* 24:2180–2193. <https://doi.org/10.1016/j.quascirev.2005.01.016>
- 1133 Masson DG, Watts AB, Gee MJR et al (2002) Slope failures on the flanks of the western Canary Islands.
1134 *Earth-Science Rev* 57:1–35. [https://doi.org/10.1016/S0012-8252\(01\)00069-1](https://doi.org/10.1016/S0012-8252(01)00069-1)
- 1135 Masson DG, Harbitz CB, Wynn RB et al (2006) Submarine landslides: processes, triggers and hazard pre-
1136 diction. *Philos Trans R Soc London A Math Phys Eng Sci* 364:2009–2039. <https://doi.org/10.1098/rsta.2006.1810>
- 1137
- 1138 McAdoo BG, Pratson LF, Orange DL (2000) Submarine landslide geomorphology, US continental slope.
1139 *Mar Geol* 169:103–136. [https://doi.org/10.1016/S0025-3227\(00\)00050-5](https://doi.org/10.1016/S0025-3227(00)00050-5)
- 1140 McAdoo BG, Moore A, Baumwoll J (2009) Indigenous knowledge and the near field population response
1141 during the 2007 Solomon Islands tsunami. *Nat Hazards* 48:73–82. <https://doi.org/10.1007/s11069-008-9249-z>
- 1142
- 1143 McAdoo BG, Ah-Leong JS, Bell L et al (2011) Coral reefs as buffers during the 2009 South Pacific tsunami,
1144 Upolu Island, Samoa. *Earth-Science Rev* 107:147–155. <https://doi.org/10.1016/j.earscirev.2010.11.005>
- 1145
- 1146 McGregor BA, Rothwell RG, Kenyon NH, Twichell DC (1993) Salt tectonics and slope failure in an area of
1147 salt domes in the northwestern Gulf of Mexico. In: *Submarine landslides: selected studies in the US*
1148 *Exclusive Economic Zone*. US Geological Survey Bulletin, pp 92–96

Natural Hazards

- 1149 McMurtry GM, Watts P, Fryer GJ et al (2004) Giant landslides, mega-tsunamis, and paleo-sea level in the
1150 Hawaiian Islands. *Mar Geol* 203:219–233. [https://doi.org/10.1016/S0025-3227\(03\)00306-2](https://doi.org/10.1016/S0025-3227(03)00306-2)
- 1151 Meyer M, Geersen J, Krastel S et al (2012) Dakar slide offshore senegal, NW-Africa: interaction of stacked
1152 giant mass wasting events and canyon evolution. In: Yamada Y, Kawamura K, Ikehara K et al (eds)
1153 Submarine mass movements and their consequences. Springer, Netherlands, Dordrecht, pp 177–188
- 1154 Monismith SG, Herdman LMM, Ahmerkamp S, Hench JL (2013) Wave transformation and wave-
1155 driven flow across a steep coral reef. *J Phys Oceanogr* 43:1356–1379. [https://doi.org/10.1175/
1156 JPO-D-12-0164.1](https://doi.org/10.1175/JPO-D-12-0164.1)
- 1157 Moore JG, Clague DA (2002) Mapping the Nuanu and Wailau landslides in Hawaii. *Hawaiian Volcanoes*
1158 *Deep Underw Perspect* 128:223–244. <https://doi.org/10.1029/GM128p0223>
- 1159 Moore DG, Curry JR, Emmel FJ (1976) Large submarine slide (olistostrome) associated with Sunda
1160 Arc subduction zone, northeast Indian Ocean. *Mar Geol* 21:211–226. [https://doi.org/10.1016/0025-
1161 3227\(76\)90060-8](https://doi.org/10.1016/0025-3227(76)90060-8)
- 1162 Moore JG, Clague DA, Holcomb RT et al (1989) Prodigious submarine landslides on the Hawaiian Ridge. *J*
1163 *Geophys Res Solid Earth* 94:17465–17484. <https://doi.org/10.1029/JB094iB12p17465>
- 1164 Moore GF, Strasser M (2016) large mass transport deposits in kumano basin, Nankai trough, Japan. In:
1165 Lamarche G, Mountjoy J, Bull S et al (eds) Submarine mass movements and their consequences: 7th
1166 international symposium. Springer International Publishing, Cham, pp 371–379
- 1167 Mori N, Takahashi T, Yasuda T, Yanagisawa H (2011) Survey of 2011 Tohoku earthquake tsunami inunda-
1168 tion and run-up. *Geophys Res Lett* 38:6–11. <https://doi.org/10.1029/2011GL049210>
- 1169 Moscardelli L, Wood L (2008) New classification system for mass transport complexes in offshore Trinidad.
1170 *Basin Res* 20:73–98. <https://doi.org/10.1111/j.1365-2117.2007.00340.x>
- 1171 Moscardelli L, Wood L (2016) Morphometry of mass-transport deposits as a predictive tool. *Bull Geol Soc*
1172 *Am* 128:47–80. <https://doi.org/10.1130/B31221.1>
- 1173 Moscardelli L, Wood L, Mann P (2006) Mass-transport complexes and associated processes in the offshore
1174 area of Trinidad and Venezuela. *Am Assoc Pet Geol Bull* 90:1059–1088. [https://doi.org/10.1306/
1175 02210605052](https://doi.org/10.1306/02210605052)
- 1176 Mosher DC, Xu Z, Shimeld J (2010) The Pliocene shelburne mass-movement and consequent tsunami,
1177 Western Scotian Slope BT - Submarine mass movements and their consequences. In: Mosher DC,
1178 Shipp RC, Moscardelli L, et al. (eds) Springer Netherlands, Dordrecht, pp 765–775
- 1179 Mountjoy JJ, McKean J, Barnes PM, Pettinga JR (2009) Terrestrial-style slow-moving earthflow kinematics
1180 in a submarine landslide complex. *Mar Geol* 267:114–127. [https://doi.org/10.1016/j.margeo.2009.09.
1181 007](https://doi.org/10.1016/j.margeo.2009.09.007)
- 1182 Mountjoy JJ, Micallef A (2012) Polyphase emplacement of a 30 km3 blocky debris avalanche and its role in
1183 slope-gully development. In: Yamada Y, Kawamura K, Ikehara K et al (eds) Submarine mass move-
1184 ments and their consequences. Springer, Netherlands, Dordrecht, pp 213–222
- 1185 Mullins HT, Dolan J, Breen N et al (1991) Retreat of carbonate platforms: response to tectonic processes.
1186 *Geology* 19:1089–1092. [https://doi.org/10.1130/0091-7613\(1991\)019%3c1089:ROCPRT%3e2.3.
1187 CO;2](https://doi.org/10.1130/0091-7613(1991)019%3c1089:ROCPRT%3e2.3.CO;2)
- 1188 Nagai R, Takabatake T, Esteban M et al (2020) Tsunami risk hazard in Tokyo Bay: the challenge of future
1189 sea level rise. *Int J Disaster Risk Reduct* 45:101321. <https://doi.org/10.1016/j.ijdrr.2019.101321>
- 1190 Nelson RC (1996) Hydraulic roughness of coral reef platforms. *Appl Ocean Res* 18:265–274. [https://doi.
1191 org/10.1016/S0141-1187\(97\)00006-0](https://doi.org/10.1016/S0141-1187(97)00006-0)
- 1192 Newton CS, Shipp RC, Mosher DC, Wach GD (2004) Importance of mass transport complexes in the Qua-
1193 ternary development of the Nile Fan, Egypt. In: Offshore Technology Conference. Offshore Technol-
1194 ogy Conference, Houston, Texas
- 1195 Nielsen P (1992) Coastal bottom boundary layers and sediment transport. World Scientific, Singapore
- 1196 Niemi TM, Ben-Avraham Z, Hartnady CJH, Reznikov M (2000) Post-Eocene seismic stratigraphy of the
1197 deep ocean basin adjacent to the southeast African continental margin: a record of geostrophic bottom
1198 current systems. *Mar Geol* 162:237–258. [https://doi.org/10.1016/S0025-3227\(99\)00062-6](https://doi.org/10.1016/S0025-3227(99)00062-6)
- 1199 Nistor I, Palermo D, Nouri Y, et al (2009) Tsunami-Induced Forces on Structures. In: Kim YC (ed) Hand-
1200 book of Coastal and Ocean Engineering. World Scientific, pp 261–286
- 1201 National Geophysical Data Center / World Data Service (2020) Global Historical Tsunami Database.
1202 NOAA National Centers for Environmental Information
- 1203 National Tsunami Hazard Mitigation Program (NTHMP) (2012) Proceedings and results of the 2011
1204 NTHMP model benchmarking workshop. US Dept. of Commerce, NOAA, and NTHMP Boulder, CO
- 1205 Normark WR, Gutmacher CE (1988) Sur submarine slide, monterey fan, central California. *Sedimentology*
1206 35:629–647. <https://doi.org/10.1111/j.1365-3091.1988.tb01241.x>

- 1207 Nott J (1997) Extremely high-energy wave deposits inside the great barrier reef, Australia: determin-
1208 ing the cause-tsunami or tropical cyclone. *Mar Geol* 141:193–207. <https://doi.org/10.1016/S0025->
1209 [3227\(97\)00063-7](https://doi.org/10.1016/S0025-3227(97)00063-7)
- 1210 Nouri Y, Nistor I, Palermo DAN, Cornett A (2010) Experimental investigation of tsunami impact on free
1211 standing structures. *Coast Eng J* 52:43–70. <https://doi.org/10.1142/S0578563410002117>
- 1212 Nygård A, Sejrup HP, Hafidason H, Bryn P (2005) The glacial North Sea Fan, southern Norwegian
1213 Margin: architecture and evolution from the upper continental slope to the deep-sea basin. *Mar Pet*
1214 *Geol* 22:71–84. <https://doi.org/10.1016/j.marpetgeo.2004.12.001>
- 1215 Okada Y (1985) Surface deformation due to shear and tensile faults in a half-space. *Bull Seismol Soc*
1216 *Am* 75:1135–1154
- 1217 Omira R, Ramalho I, Terrinha P et al (2016) Deep-water seamounts, a potential source of tsunami gener-
1218 ated by landslides? the Hironnelle Seamount, NE Atlantic. *Mar Geol* 379:267–280. <https://doi.org/>
1219 [10.1016/j.margeo.2016.06.010](https://doi.org/10.1016/j.margeo.2016.06.010)
- 1220 Omosanya KO, Alves TM (2013) A 3-dimensional seismic method to assess the provenance of mass-
1221 transport deposits (MTDs) on salt-rich continental slopes (Espírito Santo Basin, SE Brazil). *Mar*
1222 *Pet Geol* 44:223–239. <https://doi.org/10.1016/j.marpetgeo.2013.02.006>
- 1223 Owen M, Day S, Maslin M (2007) Late Pleistocene submarine mass movements: occurrence and causes.
1224 *Quat Sci Rev* 26:958–978. <https://doi.org/10.1016/j.quascirev.2006.12.011>
- 1225 Owen M, Day S, Long D, Maslin M (2010) Investigations on the peach 4 debris, a late pleistocene mass
1226 movement on the Northwest British continental margin. In: Mosher DC, Shipp RC, Moscardelli L
1227 et al (eds) *Submarine mass movements and their consequences*. Springer, Netherlands, Dordrecht,
1228 pp 301–311
- 1229 Papadopoulos GA, Gràcia E, Urgeles R et al (2014) Historical and pre-historical tsunamis in the Medi-
1230 terranean and its connected seas: geological signatures, generation mechanisms and coastal
1231 impacts. *Mar Geol* 354:81–109. <https://doi.org/10.1016/j.margeo.2014.04.014>
- 1232 Piper DJW, Aksu AE (1987) The source and origin of the 1929 grand banks turbidity current inferred
1233 from sediment budgets. *Geo-Marine Lett* 7:177–182. <https://doi.org/10.1007/BF02242769>
- 1234 Piper DJW, Pirmez C, Manley PL, et al (1997) Mass-transport deposits of the Amazon Fan. In: *Proceed-*
1235 *ings of the Ocean Drilling Program, Scientific Results*. Ocean Drilling Program, College Station,
1236 Texas, pp 109–146
- 1237 Power HE, Clarke SL, Wilson O, Hubble TTCT (2015) Tsunami hazard from submarine landslides: 3D
1238 numerical modelling in New South Wales, Australia. In: *Australasian Coasts & Ports Conference*
1239 *2015: 22nd Australasian Coastal and Ocean Engineering Conference and the 15th Australasian*
1240 *Port and Harbour Conference*. Engineers Australia and IPENZ, p 696
- 1241 Puga-Bernabéu Á, Webster JM, Beaman RJ, Guilbaud V (2011) Morphology and controls on the evolu-
1242 tion of a mixed carbonate–siliciclastic submarine canyon system, Great Barrier Reef margin,
1243 north-eastern Australia. *Mar Geol* 289:100–116. <https://doi.org/10.1016/j.margeo.2011.09.013>
- 1244 Puga-Bernabéu Á, Webster JM, Beaman RJ (2013) Potential collapse of the upper slope and tsunami
1245 generation on the great barrier reef margin, north-eastern Australia. *Nat Hazards* 66:557–575.
1246 <https://doi.org/10.1007/s11069-012-0502-0>
- 1247 Puga-Bernabéu Á, Webster JM, Beaman RJ, Guilbaud V (2013) Variation in canyon morphology on the
1248 great barrier reef margin, north-eastern Australia: the influence of slope and barrier reefs. *Geo-*
1249 *morphology* 191:35–50. <https://doi.org/10.1016/j.geomorph.2013.03.001>
- 1250 Puga-Bernabéu Á, Beaman RJ, Webster JM et al (2016) Gloria Knolls slide: a prominent submarine
1251 landslide complex on the great barrier reef margin of north-eastern Australia. *Mar Geol* 385:68–
1252 83. <https://doi.org/10.1016/j.margeo.2016.12.008>
- 1253 Puga-Bernabéu Á, Webster JM, Beaman RJ, et al. (2019) Submarine Landslides Along the Mixed Silici-
1254 clastic-Carbonate Margin of the Great Barrier Reef (Offshore Australia). In: *Submarine Land-*
1255 *slides*. American Geophysical Union, pp 313–337
- 1256 Quataert E, Storlazzi C, van Rooijen A et al (2015) The influence of coral reefs and climate change on
1257 wave-driven flooding of tropical coastlines. *Geophys Res Lett* 42:6407–6415. [https://doi.org/10.](https://doi.org/10.1002/2015GL064861)
1258 [1002/2015GL064861](https://doi.org/10.1002/2015GL064861)
- 1259 Ratzov G, Collot J-Y, Sosson M, Migeon S (2010) Mass-transport deposits in the northern Ecuador
1260 subduction trench: result of frontal erosion over multiple seismic cycles. *Earth Planet Sci Lett*
1261 296:89–102. <https://doi.org/10.1016/j.epsl.2010.04.048>
- 1262 Reeder MS, DA Stow V, Rothwell RG (2002) Late Quaternary turbidite input into the east Mediterra-
1263 nean basin: new radiocarbon constraints on climate and sea-level control. *Geol Soc London, Spec*
1264 *Publ* 191:267–278

- 1265 Rodriguez NM, Paull CK (2000) 32. DATA REPORT: 14C dating of sediment of the uppermost cape fear
1266 slide plain: constraints on the timing of this massive submarine landslide. Proc Ocean Drill Program
1267 Sci Results 164:325–332
- 1268 Rodriguez M, Chamot-Rooke N, Hébert H et al (2013) Owen Ridge deep-water submarine landslides: impli-
1269 cations for tsunami hazard along the Oman coast. Nat Hazards Earth Syst Sci 13:417–424. <https://doi.org/10.5194/nhess-13-417-2013>
- 1270 Roeber V, Yamazaki Y, Cheung KF (2010) Resonance and impact of the 2009 Samoa tsunami around
1271 Tutuila, American Samoa. Geophys Res Lett 37:1–8. <https://doi.org/10.1029/2010GL044419>
- 1272 Roger J, Dudson B, Krien Y, Zahibo N (2014) Discussion about tsunami interaction with fringing coral reef.
1273 In: Tsunami Events and Lessons Learned. Springer, pp 161–176
- 1274 Rogers JS, Monismith SG, Kowalik DA, Dunbar RB (2016) Wave dynamics of a Pacific atoll with high fric-
1275 tional effects. J Geophys Res Ocean 121:350–367. <https://doi.org/10.1002/2015JC011170>
- 1276 Rosman JH, Hench JL (2011) A framework for understanding drag parameterizations for coral reefs. J Geo-
1277 phys Res Ocean 116:C08025. <https://doi.org/10.1029/2010JC006892>
- 1278 Rothwell RG, Thomson J, Kahler G (1998) Low-sea-level emplacement of a very large Late Pleistocene
1279 “megaturbidite” in the western Mediterranean Sea. Nature 392:377–380. <https://doi.org/10.1038/32871>
- 1280 San Pedro L, Babonneau N, Gutscher M-A, Cattaneo A (2016) Origin and chronology of the Augias deposit
1281 in the Ionian Sea (Central Mediterranean Sea), based on new regional sedimentological data. Mar
1282 Geol 384:199–213. <https://doi.org/10.1016/j.margeo.2016.05.005>
- 1283 Satake K (2007) Volcanic origin of the 1741 Oshima-Oshima tsunami in the Japan Sea. Earth Planets Sp
1284 59:381–390. <https://doi.org/10.1186/BF03352698>
- 1285 Satake K, Smith JR, Shinozaki K (2002) Three-Dimensional Reconstruction and Tsunami Model of the
1286 Nuuanu and Wailau Giant Landslides, Hawaii. In: Hawaiian Volcanoes: Deep Underwater Perspec-
1287 tives. Washington DC American Geophysical Union Geophysical Monograph Series, pp 333–346
- 1288 Sayago-Gil M, Long D, Hitchen K et al (2010) Evidence for current-controlled morphology along the west-
1289 ern slope of Hatton Bank (Rockall Plateau, NE Atlantic Ocean). Geo-Marine Lett 30:99–111. <https://doi.org/10.1007/s00367-009-0163-5>
- 1290 Schambach L, Grilli ST, Kirby JT, Shi F (2018) Landslide tsunami hazard along the upper US East coast:
1291 effects of slide deformation, bottom friction, and frequency dispersion. Pure Appl Geophys 176:1–40.
1292 <https://doi.org/10.1007/s00024-018-1978-7>
- 1293 Schnyder JSD, Eberli GP, Kirby JT et al (2016) Tsunamis caused by submarine slope failures along western
1294 Great Bahama Bank. Sci Rep 6:1–9. <https://doi.org/10.1038/srep35925>
- 1295 Schwab WC, Danforth WW, Scanlon KM, Masson DG (1991) A giant submarine slope failure on the
1296 northern insular slope of Puerto Rico. Mar Geol 96:237–246. [https://doi.org/10.1016/0025-3227\(91\)90149-X](https://doi.org/10.1016/0025-3227(91)90149-X)
- 1297 Schwab JM, Krastel S, Grün M et al (2012) Submarine mass wasting and associated tsunami risk offshore
1298 western Thailand, Andaman Sea, Indian Ocean. Nat Hazards Earth Syst Sci 12:2609. <https://doi.org/10.5194/nhess-12-2609-2012>
- 1299 Shao K, Liu W, Gao Y, Ning Y (2019) The influence of climate change on tsunami-like solitary wave inun-
1300 dation over fringing reefs. J Integr Environ Sci 16:71–88. <https://doi.org/10.1080/1943815X.2019.1614071>
- 1301 Sheppard C, Dixon DJ, Gourlay M et al (2005) Coral mortality increases wave energy reaching shores pro-
1302 tected by reef flats: examples from the Seychelles. Estuar Coast Shelf Sci 64:223–234. <https://doi.org/10.1016/j.ecss.2005.02.016>
- 1303 Shi F, Kirby JT, Harris JC et al (2012) A high-order adaptive time-stepping TVD solver for Boussinesq
1304 modeling of breaking waves and coastal inundation. Ocean Model 43–44:36–51. <https://doi.org/10.1016/j.ocemod.2011.12.004>
- 1305 Shi F, Kirby JT, Tehranirad B, et al (2016) FUNWAVE-TVD fully nonlinear Boussinesq wave model with
1306 TVD solver - documentation and user’s manual (Version 3.0). Center for Applied Coastal Research,
1307 University of Delaware. Report No.: CACR-11–03
- 1308 Smith BM, Deptuck ME, Kendell KL (2010) Upper cretaceous mass transport systems above the Wyandot
1309 formation chalk, offshore Nova Scotia. In: Mosher DC, Shipp C, Moscardelli L et al (eds) Submarine
1310 mass movements and their consequences. Springer, Advances in Natural and Technological Hazards
1311 Research, Kluger-Springer Book Series, pp 605–616
- 1312 Solheim A, Berg K, Forsberg CF, Bryn P (2005) The Storegga Slide complex: repetitive large scale sliding
1313 with similar cause and development. Mar Pet Geol 22:97–107. <https://doi.org/10.1016/j.marpetgeo.2004.10.013>
- 1314 Spalding MD, Brown BE (2015) Warm-water coral reefs and climate change. Science 350:769–771. <https://doi.org/10.1126/science.aad0349>

- 1325 Spalding MD, Ruffo S, Lacambra C et al (2014) The role of ecosystems in coastal protection: adapting to cli-
1326 mate change and coastal hazards. *Ocean Coast Manag* 90:50–57. [https://doi.org/10.1016/j.ocecoaman.](https://doi.org/10.1016/j.ocecoaman.2013.09.007)
1327 [2013.09.007](https://doi.org/10.1016/j.ocecoaman.2013.09.007)
- 1328 Storlazzi CD, Gingerich SB, van Dongeren A, et al (2018) Most atolls will be uninhabitable by the mid-21st
1329 century because of sea-level rise exacerbating wave-driven flooding. *Sci Adv* 4:eaa9741. [https://doi.org/](https://doi.org/10.1126/sciadv.aap9741)
1330 [10.1126/sciadv.aap9741](https://doi.org/10.1126/sciadv.aap9741)
- 1331 Synolakis CE, Bardet J-P, Borrero JC et al (2002) The slump origin of the 1998 Papua New Guinea Tsunami.
1332 *Proc R Soc A Math Phys Eng Sci* 458:763–789. <https://doi.org/10.1098/rspa.2001.0915>
- 1333 Talukder AR, Völker D (2014) The tsunami generation potential of shovel and bulli slides in the continental
1334 margin SE Australia BT - submarine mass movements and their consequences: 6th International sym-
1335 posium. In: Behrmann J-H, Völker D et al (eds) *Krastel S. Springer International Publishing, Cham*, pp
1336 539–548
- 1337 Tappin DR, Matsumoto T, Watts P et al (1999) Sediment slump likely caused 1998 Papua New Guinea tsunami.
1338 *Eos Trans Am Geophys Union* 80:329–340. <https://doi.org/10.1029/99EO00241>
- 1339 Tappin DR, Watts P, Grilli ST (2008) The Papua New Guinea tsunami of 17 July 1998: anatomy of a cata-
1340 strophic event. *Nat Hazards Earth Syst Sci* 8:243–266
- 1341 Tappin DR, Grilli ST, Harris JC et al (2014) Did a submarine landslide contribute to the 2011 Tohoku tsunami?
1342 *Mar Geol* 357:344–361. <https://doi.org/10.1016/j.margeo.2014.09.043>
- 1343 Tehraniad B, Kirby JT, Ma G, Shi F (2012) Tsunami benchmark results for nonhydrostatic wave model
1344 NHWAVE (Version 1.1). Research Report No. CACR-11–02. Newark
- 1345 Tehraniad B, Harris JC, Grilli AR et al (2015) Far-field tsunami impact in the North Atlantic basin from large
1346 scale flank collapses of the Cumbre Vieja Volcano, La Palma. *Pure Appl Geophys* 172:3589–3616
- 1347 Ten Brink US, Geist EL, Andrews BD (2006) Size distribution of submarine landslides and its implication
1348 to tsunami hazard in Puerto Rico. *Geophys Res Lett* 33:L11307. <https://doi.org/10.1029/2006GL026125>
- 1349 Torelli L, Sartori R, Zitellini N (1997) The giant chaotic body in the Atlantic Ocean off Gibraltar: new results
1350 from a deep seismic reflection survey. *Mar Pet Geol* 14:125–134. [https://doi.org/10.1016/S0264-](https://doi.org/10.1016/S0264-8172(96)00060-8)
1351 [8172\(96\)00060-8](https://doi.org/10.1016/S0264-8172(96)00060-8)
- 1352 Urgeles R, Lastras G, Canals M et al (2003) The big '95 debris flow and adjacent unfailed sediments in the NW
1353 mediterranean sea: geotechnical sedimentological properties, and dating. In: Locat J, Mienert J, Boisvert
1354 L (eds) *Submarine mass movements and their consequences: 1st international symposium*. Springer,
1355 Netherlands, Dordrecht, pp 479–487
- 1356 Urgeles R, Leynaud D, Lastras G et al (2006) Back-analysis and failure mechanisms of a large submarine slide
1357 on the Ebro slope, NW Mediterranean. *Mar Geol* 226:185–206. [https://doi.org/10.1016/j.margeo.2005.](https://doi.org/10.1016/j.margeo.2005.10.004)
1358 [10.004](https://doi.org/10.1016/j.margeo.2005.10.004)
- 1359 Urlaub M, Talling PJ, Masson DG (2013) Timing and frequency of large submarine landslides: implications for
1360 understanding triggers and future geohazard. *Quat Sci Rev* 72:63–82. [https://doi.org/10.1016/j.quascirev.](https://doi.org/10.1016/j.quascirev.2013.04.020)
1361 [2013.04.020](https://doi.org/10.1016/j.quascirev.2013.04.020)
- 1362 Uslu B, Titov VV, Eble M, Chamberlin CD (2010) Tsunami hazard assessment for Guam. NOAA Pacific
1363 Marine Environmental Laboratory Special Rep, National Oceanic and Atmospheric Administration,
1364 Seattle, WA, USA
- 1365 Van Weering TCE, Nielsen T, Kenyon NH et al (1998) Sediments and sedimentation at the NE Faeroe con-
1366 tinental margin; contourites and large-scale sliding. *Mar Geol* 152:159–176. [https://doi.org/10.1016/](https://doi.org/10.1016/S0025-3227(98)00069-3)
1367 [S0025-3227\(98\)00069-3](https://doi.org/10.1016/S0025-3227(98)00069-3)
- 1368 Vizcaino A, Gràcia E, Pallàs R et al (2006) Sedimentology, physical properties and age of mass transport depos-
1369 its associated with the Marques de Pombal Fault Southwest Portuguese. *Margin Nor Geol Tidsskr* 86:177
- 1370 Voight B, Le Friant A, Boudon G et al (2012) Undrained sediment loading key to long-runout submarine mass
1371 movements: evidence from the caribbean volcanic arc. In: Yamada Y, Kawamura K, Ikehara K et al (eds)
1372 *Submarine mass movements and their consequences*. Springer, Netherlands, Dordrecht, pp 417–428
- 1373 Völker D, Geersen J, Behrmann JH, Weinrebe WR (2012) Submarine mass wasting off southern central chile:
1374 distribution and possible mechanisms of slope failure at an active continental margin. In: Yamada Y,
1375 Kawamura K, Ikehara K et al (eds) *Submarine mass movements and their consequences: 5th interna-*
1376 *tional symposium*. Springer, Netherlands, Dordrecht, pp 379–389
- 1377 von Huene R, Bourgois J, Miller J, Pautot G (1989) A large tsunamogenic landslide and debris flow along the
1378 Peru Trench. *J Geophys Res Solid Earth* 94:1703–1714. <https://doi.org/10.1029/JB094iB02p01703>
- 1379 von Huene R, Ranero CR, Weinrebe W, Hinz K (2000) Quaternary convergent margin tectonics of Costa Rica,
1380 segmentation of the Cocos plate, and Central American volcanism. *Tectonics* 19:314–334. [https://doi.](https://doi.org/10.1029/1999TC001143)
1381 [org/10.1029/1999TC001143](https://doi.org/10.1029/1999TC001143)
- 1382 Vorren TO, Laberg JS, Blaume F et al (1998) The norwegian-greenland sea continental margins: morphology
1383 and late quaternary sedimentary processes and environment. *Quat Sci Rev* 17:273–302. [https://doi.org/](https://doi.org/10.1016/S0277-3791(97)00072-3)
1384 [10.1016/S0277-3791\(97\)00072-3](https://doi.org/10.1016/S0277-3791(97)00072-3)
- 1385 Wang X, Mountjoy J, Power WL et al (2016) Coupled modelling of the failure and tsunami of a submarine
1386 debris avalanche offshore central New Zealand. In: Lamarche G, Mountjoy J, Bull S et al (eds) *Submarine*

- 1387 mass movements and their consequences: 7th international symposium. Springer International Publish-
1388 ing, Cham, pp 599–606
- 1389 Ward SN, Asphaug E (2003) Asteroid impact tsunamis of 2880 March 16. *Geophys J Int* 153:F6–F10. <https://doi.org/10.1046/j.1365-246X.2003.01944.x>
- 1390
- 1391 Ward SN, Day S (2003) Ritter Island volcano—lateral collapse and the tsunamis of 1888. *Geophys J Int*
1392 154:891–902. <https://doi.org/10.1046/j.1365-246X.2003.02016.x>
- 1393 Watts P, Grilli ST, Kirby JT et al (2003) Landslide tsunami case studies using a Boussinesq model and a fully
1394 nonlinear tsunami generation model. *Nat Hazards Earth Syst Sci* 3:391–402. <https://doi.org/10.5194/nhess-3-391-2003>
- 1395
- 1396 Weaver PPE, Rothwell RG (1987) Sedimentation on the madeira abyssal plain over the last 300 000 years. *Geol*
1397 *Soc London Spec Publ* 31:71–86
- 1398 Webster JM, Davies PJ, Beaman RJ et al (2008) Evolution of drowned shelf edge reefs in the GBR; implications
1399 for understanding abrupt climate change, coral reef response and modern deep water benthic habitats—
1400 RV Southern Surveyor—voyage summary. Tasmania, Marine National Facility, Hobart, p 18
- 1401 Webster JM, George NPJ, Beaman RJ et al (2016) Submarine landslides on the Great Barrier Reef shelf edge
1402 and upper slope: a mechanism for generating tsunamis on the north-east Australian coast? *Mar Geol*
1403 371:120–129. <https://doi.org/10.1016/j.margeo.2015.11.008>
- 1404 Wei Y, Fritz HM, Titov VV et al (2015) Source models and near-field impact of the 1 april 2007 solomon
1405 islands tsunami. *Pure Appl Geophys* 172:657–682. <https://doi.org/10.1007/s00024-014-1013-6>
- 1406 Wien K, Kölling M, Schulz HD (2007) Age models for the cape blanc debris flow and the mauritania slide com-
1407 plex in the atlantic Ocean off NW Africa. *Quat Sci Rev* 26:2558–2573. <https://doi.org/10.1016/j.quascirev.2007.06.018>
- 1408
- 1409 Wild C, Hoegh-Guldberg O, Naumann MS et al (2011) Climate change impedes scleractinian corals as primary
1410 reef ecosystem engineers. *Mar Freshw Res* 62:205–215. <https://doi.org/10.1071/MF10254>
- 1411 Williams SP, Davies TR, Barrows TT et al (2014) Flank-collapse on Ta'u Island, Samoan archipelago: timing
1412 and hazard implications. In: Sassa K, Canuti P, Yin Y (eds) *Landslide science for a safer geoenvironment*.
1413 Springer International Publishing, Cham, pp 583–588
- 1414 Winkelmann D, Geissler W, Schneider J, Stein R (2008) Dynamics and timing of the hinlopen/yermaak
1415 megaslide north of spitsbergen, arctic Ocean. *Mar Geol* 250:34–50. <https://doi.org/10.1016/j.margeo.2007.11.013>
- 1416
- 1417 Wynn RB, Masson DG, Stow DA, Weaver PP (2000) The Northwest African slope apron: a modern analogue
1418 for deep-water systems with complex seafloor topography. *Mar Pet Geol* 17:253–265. [https://doi.org/10.1016/S0264-8172\(99\)00014-8](https://doi.org/10.1016/S0264-8172(99)00014-8)
- 1419
- 1420 Wynn RB, Talling PJ, Masson DG et al (2010) Investigating the timing, processes and deposits of one of the
1421 world's largest submarine gravity flows: the 'bed 5 event' off Northwest Africa. In: Mosher DC, Shipp
1422 RC, Moscardelli L et al (eds) *Submarine mass Movements and their consequences*. Springer, Nether-
1423 lands, Dordrecht, pp 463–474
- 1424 Xing HL, Ding RW, Yuen D (2015) Tsunami hazards along the eastern Australian coast from potential earth-
1425 quakes: results from numerical simulations. *Pure Appl Geophys* 172:2087–2115. <https://doi.org/10.1007/s00024-014-0904-x>
- 1426
- 1427 Yao Y, Huang Z, Monismith SG, Lo EYM (2012) 1DH Boussinesq modeling of wave transformation over
1428 fringing reefs. *Ocean Eng* 47:30–42. <https://doi.org/10.1016/j.oceaneng.2012.03.010>
- 1429 Yongfu S, Bolin H (2014) A potential tsunami impact assessment of submarine landslide at Baiyun depres-
1430 sion in Northern South China Sea. *Geoenvironmental Disasters* 1:7. <https://doi.org/10.1186/s40677-014-0007-0>
- 1431
- 1432 Young IR (1989) Wave transformation over coral reefs. *J Geophys Res Ocean* 94:9779–9789. <https://doi.org/10.1029/JC094iC07p09779>
- 1433
- 1434 Young IR, Hardy TA (1993) Measurement and modelling of tropical cyclone waves in the great barrier reef.
1435 *Coral Reefs* 12:85–95. <https://doi.org/10.1007/BF00302108>

1436 **Publisher's Note** Springer Nature remains neutral with regard to jurisdictional claims in published maps and
1437 institutional affiliations.

1438

Authors and Affiliations

Amanda C. Thran¹  · Sascha Brune^{2,3}  · Jody M. Webster⁴  ·
Dale Dominey-Howes⁵  · Daniel Harris⁶ 

- ¹ Water Research Laboratory, School of Civil and Environmental Engineering, University of New South Wales, Sydney, NSW 2052, Australia
- ² GFZ German Research Centre for Geosciences, Telegrafenberg, 14473 Potsdam, Germany
- ³ Institute of Geosciences, University of Potsdam, Potsdam, Germany
- ⁴ Geocoastal Research Group, School of Geosciences, University of Sydney, Sydney, NSW 2050, Australia
- ⁵ Asia-Pacific Natural Hazards and Disaster Risk Research Group, School of Geosciences, University of Sydney, Sydney, NSW 2050, Australia
- ⁶ School of Earth and Environmental Sciences, University of Queensland, Brisbane, QLD 4072, Australia

UNCORRECTED PROOF

Journal:	11069
Article:	4686

Author Query Form

Please ensure you fill out your response to the queries raised below and return this form along with your corrections

Dear Author

During the process of typesetting your article, the following queries have arisen. Please check your typeset proof carefully against the queries listed below and mark the necessary changes either directly on the proof/online grid or in the 'Author's response' area provided below

Query	Details Required	Author's Response
AQ1	Please note that the figures are renumbered to ensure sequential order of citations. Kindly check and confirm the change.	
AQ2	Kindly check and confirm the inserted Figure 17 citation is correct.	
AQ3	As References Garziglia et al., 2010 and Garziglia et al., 2010 are same, we have deleted the duplicate reference and renumbered accordingly. Please check and confirm.	